Analysis of Three-Dimensional Flow Field Inside the Pilot Stage of the Deflector Jet Servo Valve

Shuanglu Li (1710765@tongji.edu.cn)
Tongji University https://orcid.org/0000-0002-3337-0791
YaoBao Yin
Tongji University
JiaYang Yuan
Aviation Key Laboratory of Science and Technology on Aero Electromechanical System Integration
ShengRong Guo
Aviation Key Laboratory of Science and Technology on Aero Electromechanical System Integration

Original Article

Keywords: Deflector jet servo valve, Pilot stage, Three-dimensional jet, Jet expansion, Static characteristics, Numerical integration

Posted Date: May 5th, 2021

DOI: https://doi.org/10.21203/rs.3.rs-447124/v1

Title page

Analysis of Three-Dimensional Flow Field Inside the Pilot Stage of the Deflector Jet Servo Valve

Shuang-Lu Li, born in 1995, is currently a PhD candidate at *School of Mechanical Engineering, Tongji University, China*. He received his bachelor degree from *Yanshan University, China*, in 2017. His research interests include electro-hydraulic servo components.
Tel: +86-185-1218-3901; E-mail: 1710765@tongji.edu.cn

Yao-Bao Yin, born in 1965, is currently a professor at *Tongji University, China*. He received his PhD degree from *Saitama Universtiy, Japan,* in 1999. His research interests include electro-hydraulic servo system and components.
Tel: +86-137-7431-3727; E-mail: y-yin@tongji.edu.cn

Jia-Yang Yuan, born in 1992, is currently an engineer at *Nanjing Mechatronic and Hydraulic Engineering Research Centre* and *Aviation Key Laboratory of Science and Technology on Aero Electromechanical System Integration, China*.
E-mail: jiayangyuan2010@163.com

Sheng-Rong Guo, born in 1963, is currently a research fellow at *Nanjing Mechatronic and Hydraulic Engineering Research Centre* and *Aviation Key Laboratory of Science and Technology on Aero Electromechanical System Integration, China*.
E-mail: guosr@126.com

Corresponding author：Shuang-Lu Li　E-mail：1710765@tongji.edu.cn

ORIGINAL ARTICLE

Analysis of three-dimensional flow field inside the pilot stage of the deflector jet servo valve

Shuang-Lu Li[1] • Yao-Bao Yin[1] • Jia-Yang Yuan[2]• Sheng-Rong Guo[2]

Received June xx, 201x; revised February xx, 201x; accepted March xx, 201x

Abstract: Current two-dimensional flow field model has some defects in describing the pilot stage's flow field and static characteristics of the deflector jet servo valve(DJSV) because the three-dimensional(3D) jet of the flow field is ignored. In order to overcome the shortcomings, a new flow field model is proposed and the energy transfer process of the pilot stage is obtained. In this model, the flow field is divided into five regions: pressure jet region, free jet region, mixed collision region, secondary jet region and pressure recovery region. Especially, three-dimensional turbulent jet is adopted in the free jet region for the first time to describe the structure of the flow field, and the jet entrainment model is proposed in pressure recovery region to describe the coupling relationship between the pressure in the receiving chamber and the jet flow which has never been considered before. The static characteristics of the pilot stage, such as pressure-flow characteristics, pressure characteristics and flow characteristics are obtained, and the relationship between zero-position valve coefficients and the key structural parameters of the pilot stage is analyzed. The results show that main structural parameters that affect the pressure gain include the length of receiving chamber, the width of guide groove outlet and the width of the wedge; The thickness of jet-pan has the most significant influence on flow gain. The flow field structure and the static characteristics are verified respectively by finite element analysis(FEA) and experimental results, and the results show that the pilot stage mathematical model has good reliability which is beneficial to understand the working mechanism of the pilot stage provide theoretical basis for parameter optimization.

Keywords: Deflector jet servo valve • Pilot stage • Three-dimensional jet • Jet expansion • Static characteristics • Numerical integration

✉ Yao-Bao Yin
y-yin@tongji.edu.cn

[1] School of Mechanical Engineering, Tongji University, Shanghai 201804, China

[2] Nanjing Mechatronic and Hydraulic Engineering Research Centre, Aviation Key Laboratory of Science and Technology on Aero Electromechanical System Integration, Nanjing 210061, Jiangsu, China

1 Introduction

Before the second world war, servo valves began to be used in the field of fluid transmission and control in order to meet the needs of the requirement of weapons. After decades of development, electro-hydraulic servo valve now includes nozzle flapper servo valve(NFSV), jet pipe servo valve(JPSV), deflector jet servo valve(DJSV) and direct drive servo valve(DDSV)[1,2]. Servo valve has been widely used in hydraulic servo control system in aerospace, nuclear power, metallurgy and other high-end equipment. Because of the important role of servo valve, the modeling method[3], performance under extreme environment[4], structure form[5], wear[6], flow field[7,8], driven mode[9] and other aspects of it have been widely studied. Among them, DJSV has attracted great attention since its first appearance[10] due to its advantages such as simple structure, strong anti-pollution ability and failure protection mechanism. In 1970, Moog developed the two-stage DJSV and gradually popularized its use. However, since the pilot stage is the core component of the DJSV and the energy transfer process and flow field structure is very complex, there still many unsolved questions[11]. Scholars have carried out many studies in the pilot stage modeling[12-16], flow force calculation[17,18], cavitation[19] and application of new materials[20,21] on the DJSV and got rich research achievements. For example, Yin et al built a simplified model to calculate pressure characteristic based on Bernoulli equation and analyzed the null shift when the pilot stage structure is not symmetrical[12]; Yan et al established a two-dimensional(2D) model about

internal flow field of pilot stage, and obtained the steady-state fluid force by the momentum principle method and the differential pressure method based on the simulated discrete data[16]; B K Saha and Li researched the cavitation phenomena inside the pilot stage through experimental flow visualization and numerical investigations, the attached cloud-like cavitation or bubble shedding is observed and identified the significant locations of cavitation[19]; D K Sangiah and Y C Zhu developed the deflector servo valve driven by the bimorph rectangular actuator and the giant magnetostrictive actuator respectively[20,21], and analyzed the static and dynamic characteristics of the servo valve. In the research topic of the DJSV, the modeling of the pilot stage has become a hot research issue in recent years. Related modeling methods can be mainly classified into the following categories:

The first type aims at the pilot stage whose guide groove is circle, modeling the pressure characteristics based on axisymmetric jet theory and Bernoulli's theorem or momentum theorem[12,13]. The second and third type aims at the pilot stage whose guide groove is rectangular. The second method ignores the influence of the thickness of the jet-pan on the flow field and considers the flow as a plane jet, modeling and analysis are carried out based on plane jet theory and parameter correction[14]. In the third method, the rectangular jet is regarded as a plane jet with a certain thickness, which is equal to the thickness of the jet-pan. On this basis, the pressure characteristics and flow characteristics are modeled, but the entrainment of the jet in the third dimension is also ignored[15,16]. In terms of research objects, since typical jet nozzle, guide groove and receiving chamber of the pilot stage are rectangular, the model calculation method based on axisymmetric jet is not suitable for most DJSV and has no general significance. From the perspective of modeling method, both the second and the third modeling methods for the rectangular guide groove are in essence researches on the simplification of the three-dimensional jet structure into the two-dimensional model structure. From the results of the study, the vast majority of studies only involves the pressure characteristics, flow characteristics and flow force of the pilot stage, but few about pressure-flow characteristics. However, pressure-flow characteristics is a much more important feature of pilot stage, which can reflect the static and dynamic performance, and its research value is more meaningful.

Aiming at the defects of the current DJSV pilot stage model, based on the theory of three-dimensional turbulent jet and the momentum conservation theorem, a flow field model of the pilot stage which is more in line with the actual state of flow field is established through reasonable assumptions. The mapping relationship between static characteristics such as pressure-flow characteristics and deflector displacement is obtained by numerical integration, and the influence of main structural parameters on pressure gain and flow gain is analyzed. This work can provide a theoretical basis for optimizing the parameters of the pilot stage of the DJSV.

2 Working Principle of the DJSV

Figure 1 shows the structure and operation principle of the DJSV. A typical pilot stage mainly includes a jet-pan, two cover plates, and a deflector which is connected to the torque motor armature component. There is a V-shaped groove on the deflector, the region between the jet-pan and the cover plates forms the pilot stage's flow field, which contains a pressure inlet, a pressure outlet and two receiving chambers. The inlet and outlet are connected with the oil supply chamber and oil return chamber of the servo valve respectively, and two receiving chambers are connected to both ends of the slide valve. When the torque motor drives the armature component to move, the deflector and guide groove deviate as well and makes the fluid flow into two receiving chambers inconsistently, resulting in different recovery pressures and drives the slide spool to move.

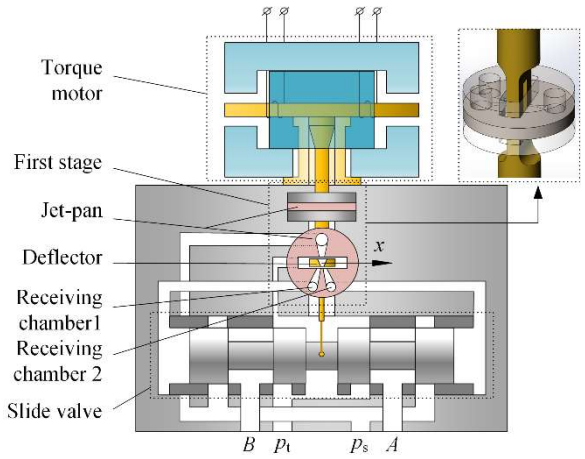

Figure 1 Working principle of the DJSV

3 Mathematical Model of the Flow Field

3.1 Partition of pilot stage's flow field

In order to have a clearer understanding about the jet flow process of the pilot stage and facilitate modeling, the pilot stage's flow field is divided into five regions as shown in Figure 2, which are as follows:

(1) Pressure jet region: the region before the jet nozzle

(region before section 1-1). In this region, fluid forms a high-speed jet and flows out of the jet nozzle driven by the pressure difference between oil supply pressure and oil return pressure.

(2) Free jet region: the region from the jet nozzle to the contact with the wall surface (the region between section 1-1 and section 2-2). In this region, the jet is unrestrained, freely expands and constantly mixes with surrounding fluid, resulting in the expansion of the jet flow.

(3) Mixed collision region: the region from the jet contact wall to the outlet of the guide groove (the region between section 2-2 and section 3-3), in this region, fluid collides with the wall of the deflector and causes energy loss.

(4) Secondary jet region: the region from the outlet of the guide groove to the plane of the receiving chamber (the region between section 3-3 and section 4-4), The fluid flows from the outlet of the guide groove and then expands freely again. Due to the difference between the outlet of the guide groove and the jet nozzle, the jet flow at this region is different from the free jet region.

(5) Pressure recovery region: the region where jet enters the receiving chambers and flows out of the receiving chambers (region after section 4-4). After entering the two receiving chambers, fluid drives the slide valve to move and maintains pressure in the receiving chambers.

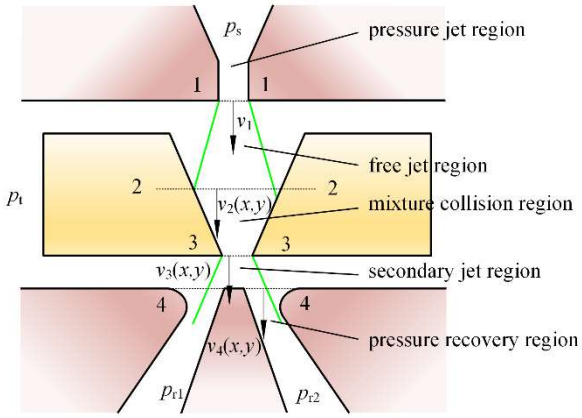

Figure 2 Flow field partition diagram

According to the above partition and fluid motion characteristics of the region, the mathematical model of flow field of each region was established respectively, and get the entire pilot stage's flow field model. Since the deflector displacement is generally very small, the modeling is only for the pilot stage's flow field of deflector under small displacement.

3.2 Pressure jet region

In this region, the high-pressure potential energy of the fluid is converted to high-speed kinetic energy. The flow velocity of the jet nozzle can be calculated by Bernoulli equation, ignoring the change of the gravitational potential energy and inflow velocity because the inlet flow area is much greater than the jet nozzle flow area, there is:

$$\frac{p_s - p_t}{\rho g} = \frac{\alpha v_1^2}{2g} + \zeta_1 \frac{v_1^2}{2g}, \tag{1}$$

where p_s refers to the oil pressure at the pressure inlet, p_t is the oil return pressure; α is the kinetic energy correction factor, 2 for laminar flow and 1 for turbulent flow, v_1 is the flow velocity of the nozzle, ζ_1 is the energy loss coefficient

$$\zeta_1 = \zeta_{1a} + \zeta_{1c} + \lambda_{1b} \frac{l_1}{L}, \tag{2}$$

where ζ_{1a} is local loss coefficient, ζ_{1c} is cavitation loss coefficient[22], λ_{1b} is coefficient of resistance loss along the way which is calculated according to empirical formula, $\lambda = 0.3164/\mathrm{Re}^{0.25}$. The Reynolds number Re of the rectangular section runner can be calculated according to the following formula

$$\mathrm{Re} = \frac{\rho v_1 L}{\mu} = \frac{2\rho v_1 ab}{\mu(a+b)}, \tag{3}$$

where μ is the dynamic viscosity of fluid, a and b are the width and height of the jet nozzle respectively. In the pilot stage, the jet velocity v_1 is as high as 200m/s, and the Reynolds number is far higher than the critical value of the jet[23], which is a fully developed turbulence, So the kinetic energy loss coefficient is 1 in formula (1)

According to the above model, the initial velocity of jet can be obtained.

3.3 Free jet region

The jet from the nozzle into the semi-infinite space of the same fluid is called free jet. As for free jet, most researches focus on axisymmetric free jet and planar free jet. When the aspect ratio of the jet nozzle is less than 5, it is called three-dimensional jet, which can be divided into three regions. They are potential core region, characteristics decay region and axisymmetric type decay region[24].

Since the distance from the jet nozzle to deflector is very short, the jet in free jet region is in the potential core region which consists of two parts, one is the constant velocity region where the velocity is consistent with the jet nozzle velocity, and the other is the shear layer whose velocity decreases due to the mixing characteristics of the jet. Due to the complexity of 3D jet, the velocity distribution lacks effective mathematical expression, but in plane jet and circular jet, the velocity distribution of shear layer has been extensively studied, and there are many velocity distribution models such as Gaussian distribution model, polynomial distribution model and cosine function model. In order to

facilitate calculation and solution, the cosine function velocity distribution of circular jet is used to simulate three-dimensional jet, as shown in Figure 3. The flow state is simplified and assumed as follows:

(1) In free jet region, the isovelocity line in the streamwise direction is rectangular and the velocity in the crossflow direction can be ignored[25];

(2) The velocity in the constant velocity region is equal to the jet nozzle velocity, the velocity distribution in the shear layer conforms to the cosine function distribution law. The shear layer boundary along the x direction is equal to the circular jet boundary with the width of jet nozzle a as the diameter; the shear layer boundary along the y direction is equal to the circular jet boundary with the jet nozzle height b as the diameter.

According to the above assumptions, there are:

The inner and outer boundaries of the shear layer along x direction d_{a1} and d_{a2} are:

$$d_{a1}=\left(0.95a-0.194L\right)/2\,, \tag{4}$$

$$d_{a2}=\left(1.07a+0.316L\right)/2\,, \tag{5}$$

The inner and outer boundaries of the shear layer along y direction d_{b1} and d_{b2} are:

$$d_{b1}=\left(0.95b-0.194L\right)/2\,, \tag{6}$$

$$d_{b2}=\left(1.07b+0.316L\right)/2\,, \tag{7}$$

In the shear layer, the velocity distribution in the shear layer is[26]

$$v_2(x,y)=\begin{cases}\dfrac{1}{2}v_1\left(1-\cos\dfrac{d_{a2}-|x|}{d_{a2}-d_{a1}}\pi\right) \\ |y|\leqslant d_{b1}+k\left(|x|-d_{a1}\right) \\ \dfrac{1}{2}v_1\left\{1-\cos\dfrac{d_{a2}-\left[\left(|y|-d_{b1}\right)/k+d_{a1}\right]}{d_{a2}-d_{a1}}\pi\right\} \\ |y|>d_{b1}+k\left(|x|-d_{a1}\right)\end{cases} \tag{8}$$

$$k=\frac{d_{b2}-d_{b1}}{d_{a2}-d_{a1}}$$

where L is the length of the free jet, that is the distance from section 1-1 to the section 2-2. As shown in Figure. 4, L and structure parameters have the following geometric relationship

$$L=L_0-x_f\cdot\cot\theta\,, \tag{9}$$

where L_0 is the length of the free jet when the deflector is at zero position, and there is

$$\frac{\left(2d_{a2}-a_n\right)}{2\tan\theta}+L_0+\frac{\left(D-d\right)}{2}=D\,, \tag{10}$$

So

$$L_0=\frac{\tan\theta\left(D+d\right)-1.07a+a_n}{\left(2\tan\theta+0.316\right)}\,, \tag{11}$$

where θ is the half-angle of the V-shaped guide groove, d is the thickness of the deflector, D is the distance from the jet nozzle to receiving chamber, a_n is the width of guide groove outlet.

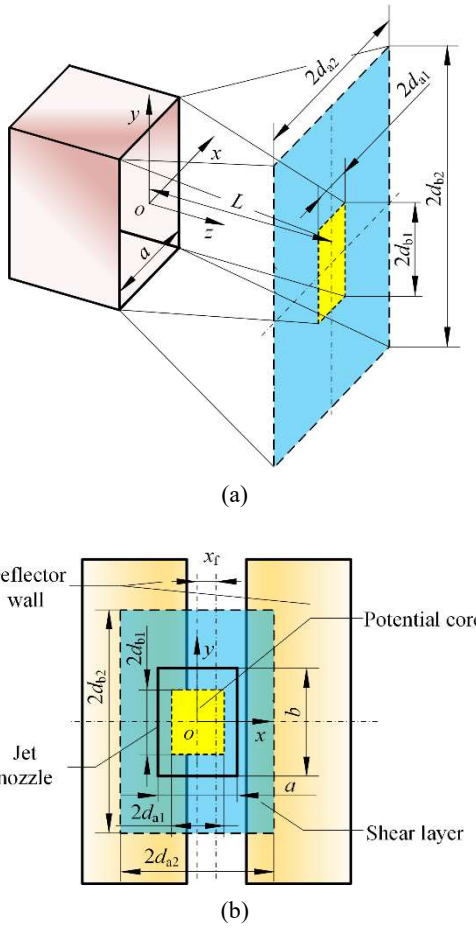

Figure 3 Schematic diagram of the free jet region

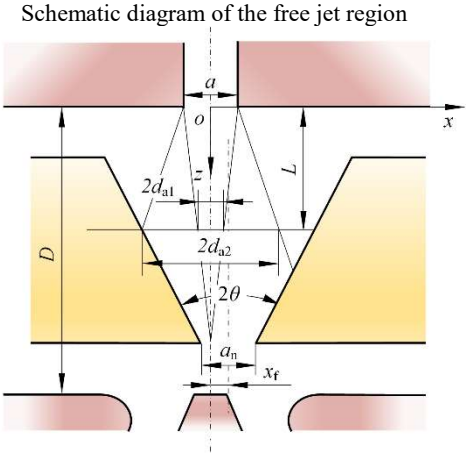

Figure 4 Structural parameters of the jet and the pilot stage

3.4 Mixed collision region

In this region, the jet flow is constrained by the guide groove, the collision between fluid flow and the guide groove results in momentum and energy loss, resulting in the destruction of the 3D free jet structure in this region. The constant velocity region of jet no longer exists. For this region, the velocity distribution at the outlet of the guide groove is concerned. Therefore, the following simplified assumptions in this region are made in combination with Figure 5.

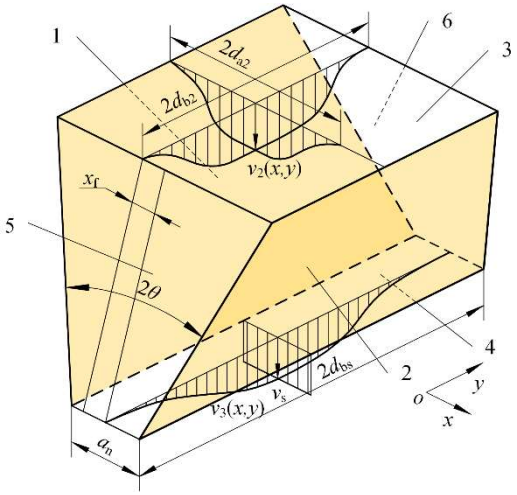

Figure 5 Schematic diagram of mixed jet region

(1) The outer boundary of the jet along y direction d_{bs} still conforms to the linear expansion law of the jet, but the inner boundary doesn't exist because the constant velocity region disappears.

(2) The velocity distribution along the y direction at the outlet of the guide groove satisfies the cosine function distribution, and the velocity distribution along the x direction is consistent.

(3) Ignore the velocity in the crossflow direction as well.

Based on above assumptions, the velocity distribution of the jet at the outlet of the guide groove can be obtained as follows:

$$v_3(x,y)=\frac{1}{2}v_s\left(1-\cos\frac{d_{bs}-y}{d_{bs}}\pi\right), \tag{12}$$

$$d_{bs}=\left[1.07b+0.316\frac{(D+d)}{2}\right]\Big/2, \tag{13}$$

where v_s is the maximum velocity at the outlet of the guide groove which can be obtained by the momentum conservation theorem as follows:

Take section 2-2, section 3-3, two deflector walls of the guide groove and the outer boundary of the jet as the control body, which is shown in Figure 5. In the streamwise direction, known by the law of conservation of momentum, the momentum difference between the flow's entering and leaving the control body is equal to the momentum loss in the collision between the fluid and the two deflector walls, namely:

$$J_i-J_o=J_{1z}+J_{2z}, \tag{14}$$

where J_i is the momentum of the fluid entering the control body, which can be calculated by integrating the velocity of section 2-2. J_o is the momentum of the fluid leaving the control body. J_{1z} and J_{2z} are the momentum lost by the collision between the fluid and the two deflector walls respectively.

As shown in Figure 6, triangle zones on both sides are respectively taken as the control bodies. Take the left control body for example, after the jet enters the guide groove from section 2-2, it flows down along the y' direction of the deflector wall and the velocity along the x' direction falls to zero. The momentum theorem in the x' direction is as follows:

$$F_1=J_1\sin\theta, \tag{15}$$

where J_1 is the momentum entering the left control body, F_1 is the flow force generated by the jet towards the wall of the guide groove.

$$J_1=\int_{A_1}\rho v_2^{\,2}(x,y)\mathrm{d}s, \tag{16}$$

where A_1 is the projected area of the left control body on plane xoy .

Therefore, it can be obtained that the momentum loss in the z direction by the collision is:

$$J_{1z}=F_1\cdot\sin\theta=\sin^2\theta\int_{A_1}\rho v_2^{\,2}(x,y)\mathrm{d}s, \tag{17}$$

Similarly, it can be obtained that momentum loss in the z direction by the collision in the right control body is:

$$J_{2z}=F_2\cdot\sin\theta=\sin^2\theta\int_{A_2}\rho v_2^{\,2}(x,y)\mathrm{d}s, \tag{18}$$

where A_2 is the projected area of the right control body on plane xoy.

The maximum velocity at the outlet of the guide groove v_s is obtained from Equations(12)~(18), and the velocity distribution at the outlet of the guide groove can be obtained through equation(12).

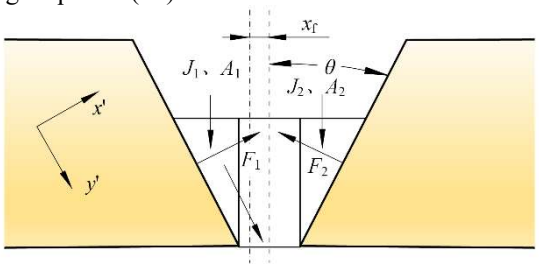

Figure 6 Schematic diagram of mixed jet region

3.5 Secondary jet region

In the secondary jet region, assuming that the jet boundary still conforms to the law of linear expansion as shown in Figure 7, the inner and outer boundaries along x direction d_{ar1} and d_{ar2} and the outer boundary along y direction d_{br2} of the shear layer can be obtained as follows:

$$\begin{aligned} d_{ar1} &= \left[0.95a_n - 0.194\frac{(D-d)}{2}\right]\Big/2 \\ d_{ar2} &= \left[1.07a_n + 0.316\frac{(D-d)}{2}\right]\Big/2 \\ d_{br2} &= (1.07b + 0.316D)/2 \end{aligned}, \tag{19}$$

The velocity distribution of section 4-4 is as follows:

$$v_4(x,y) = \begin{cases} \dfrac{1}{2}v_s\left(1-\cos\dfrac{d_{ar2}-y}{d_{ar2}}\pi\right) \\ x_f - d_{ar1} < x < x_f + d_{ar1} \\ \dfrac{1}{4}v_s\left(1-\cos\dfrac{d_{ar2}-y}{d_{ar2}}\pi\right)\left(1-\cos\dfrac{d_{ar2}-|x-x_f|}{d_{ar2}-d_{ar1}}\pi\right) \\ x_f - d_{ar2} < x < x_f - d_{ar1} \text{ or } x_f + d_{ar1} < x < x_f + d_{ar2} \end{cases}, \tag{20}$$

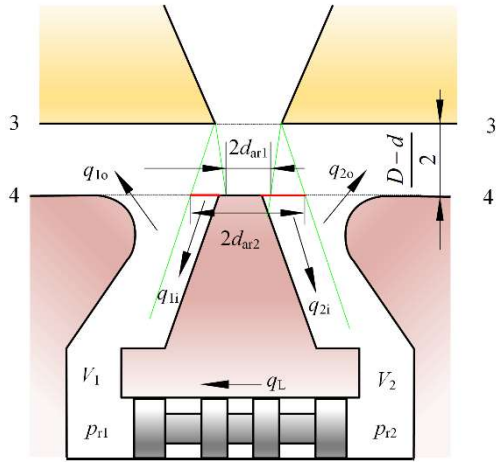

Figure 7 Schematic diagram of secondary jet region and pressure recovery region

3.6 Pressure recovery region

As shown in Figure 7, the pressure recovery region of the pilot stage is connected to both ends of the slide valve of the DJSV. The high-velocity fluid from the secondary jet enters the receiving chamber, one part is converted into flow q_L pushing the movement of the slide spool; the other part flows out of the receiving chamber under the effect of pressure difference between the inside and outside of the receiving chamber.

For two receiving chambers, there is

$$q_L = q_{1o} - q_{1i}, \tag{21}$$

$$q_L = q_{2i} - q_{2o}, \tag{22}$$

where q_{1i} and q_{2i} are flow rate into two chambers respectively. In the previous modeling, the effect of the pressure in the receiving chamber on the jet flow has never been considered, but in fact, the pressure in the receiving chamber will also affect the state of the jet flow. As shown in Figure 8, when the pressure is higher, the length of the jet is shorter and the flow into the receiving chamber is smaller; when the pressure is lower, the length of the jet is longer and the flow is larger. The jet flow and the pressure in the chamber is mutually coupled. In order to simplify the analysis, the flow rate into the chamber is divided into two parts, one is the jet flow received at 4-4 section q_{1s} and q_{2s}, the other part is the entrainment flow q_{t1} and q_{t2} after 4-4 section because of the jet expansion.

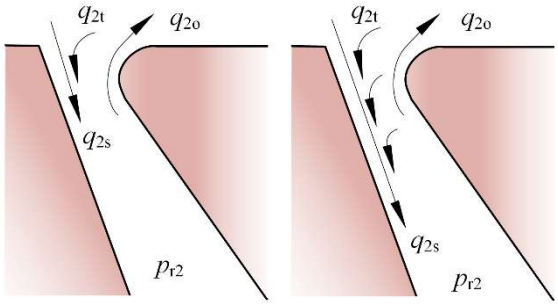

Figure 8 Schematic diagram of jet entrainment

Study has shown that the entrainment flow is related to three parameters, namely, the jet area when the deflector is at zero position, the jet flow and the recovery pressure of the receiving chamber. Specifically, the larger the jet area is, the higher the jet flow at 4-4 section is; the smaller the recovery pressure is, the higher the entrainment flow rate is . q_{1o} and q_{2o} are flow rate out of the chambers due to different pressure. By numerical integration and Bernoulli equation, there are

$$q_{1i} = q_{1s} + q_{1t} = \left(1 + \lambda\frac{p_s}{p_{r1}+p_a}\frac{A_0}{L_r b}\right)\int_{A_{1i}} v_4(x,y)\,ds, \tag{23}$$

$$q_{2i} = q_{2s} + q_{2t} = \left(1 + \lambda\frac{p_s}{p_{r2}+p_a}\frac{A_0}{L_r b}\right)\int_{A_{2i}} v_4(x,y)\,ds, \tag{24}$$

$$q_{1o} = C_d A_{1o}\sqrt{\frac{2(p_{r1}-p_0)}{\rho}}, \tag{25}$$

$$q_{2o} = C_d A_{2o}\sqrt{\frac{2(p_{r2}-p_0)}{\rho}}, \tag{26}$$

where p_{r1} and p_{r2} are the recovery pressures of the two receiving chambers, λ is the entrainment coefficient, which can be considered as a constant proportional to the thickness of the jet-pan, p_a is pressure constant, A_0 is the jet area when the deflector is at zero position, A_{1i} and A_{2i} are the inflow area of the two chambers, A_{1o} and A_{2o} are the outflow area of the two chambers. According to Figure 9, there are

$$A_{1i} = (d_{ar2} - x_f - 0.5e)b, \quad (27)$$

$$A_{2i} = (d_{ar2} + x_f - 0.5e)b, \quad (28)$$

$$A_{1o} = L_r b - A_{1i}, \quad (29)$$

$$A_{2o} = L_r b - A_{2i}, \quad (30)$$

where e is the width of the wedge, L_r is the width of the throat of the receiving chamber.

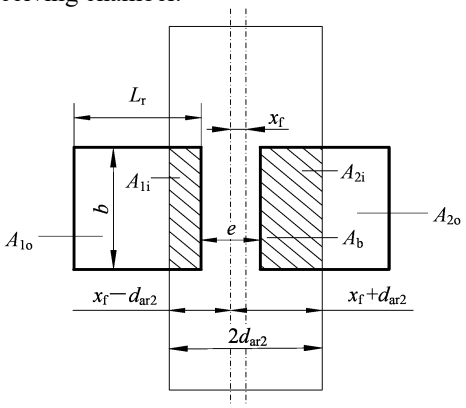

Figure 9 Structure diagram of receiving area

According to the above model, the relationship between the pressure and the flow of the two receiving chambers under different deflector positions can be obtained, and the modeling of the flow field of the pilot stage is completed.

4 Discussion on Theoretical Model

According to flow field model, the static characteristics such as pressure-flow characteristics, pressure characteristics and flow characteristics are calculated; the key structure parameters effect on the static characteristics is analyzed. The main structural parameters of the pilot stage involved and the aforementioned empirical constants are shown in Table 1.

Table 1 Structure parameters of pilot stage of the DJSV

Parameters	Value
Width of jet nozzle a(mm)	0.155
Thickness of jet-pan b(mm)	0.51
Distance from jet nozzle to receiving chamber D(mm)	1.04
Thickness of the deflector d(mm)	0.6
Width of guide groove outlet a_n(mm)	0.123
Half angle of guide groove θ(°)	18.35
Length of receiving chamber L_r(mm)	0.221
Width of the wedge e(mm)	0.1
Local loss coefficient ζ_{1a}	0.05
Cavitation loss coefficient ζ_{1c}	0.1
Entrainment coefficient λ	1.9
Pressure constant p_a (MPa)	3.5
Supply pressure p_s (MPa)	21
Return pressure p_0 (MPa)	0
flow coefficient C_d	0.85
Oil density ρ(kg/m^3)	778
Oil dynamic viscosity μ (Pa·s)	0.00114

4.1 Static characteristics of the pilot stage

(1) Pressure-flow characteristics

Pressure-flow characteristics refer to the relationship between the load pressure difference between the two chambers and the load flow through the two chambers when the deflector is in different positions. The pressure-flow characteristics curve can reflect not only the working power of the pilot stage, but also the cut-off load pressure characteristics and no load flow characteristics of the pilot stage, which is the most important static characteristics of the pilot stage. According to Equations(21) and (22), the relationship between the load flow and the flow rate of the inflow and outflow of the receiving chambers is

$$q_L = \frac{(q_{1o} - q_{2o}) - (q_{1i} - q_{2i})}{2}, \quad (31)$$

Thin-walled orifices are used to simulate the load in the pilot stage. The relationship between the load flow q_L and the load pressure p_L can be obtained.

$$q_L = C_d \frac{d_0^2}{4}\sqrt{\frac{2p_L}{\rho}}, \quad (32)$$

where d_0 is the diameter of the thin-walled orifice.

Figure 10. shows the pressure-flow characteristics of the pilot stage. It can be found that when the deflector is fixed, there is an approximate linear relationship between the load flow and the load pressure; the flow-pressure coefficient is a constant value. When the load pressure increases, the load flow basically decreases linearly. When the deflector position increases, the flow-pressure coefficient decreases slightly, but the change is not obvious.

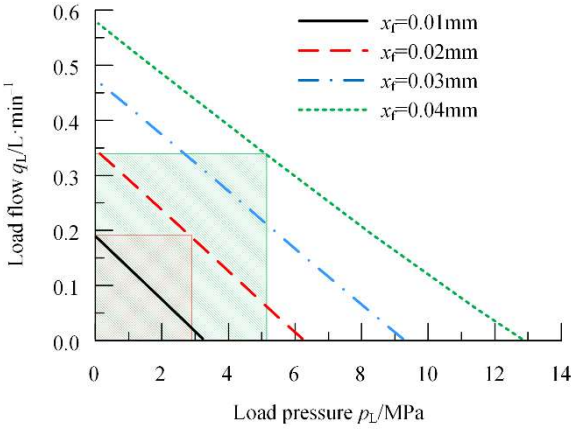

Figure 10 Pressure-flow characteristics of the pilot stage at different positions

(2) Cut-off load pressure characteristics

In Figure 10, when the load flow drops to 0, the load pressure at this point is the cut-off load pressure between the two chambers. The cut-off load pressure reflects the maximum load capacity that can be pushed by the pilot stage. It can be seen from the Figure 11 that with the increase of the deflector position, the pressure of the high-pressure chamber increases more obviously; while the pressure of the low-pressure chamber decreases and tends to be flat. The pressure difference between the two chambers is approximately linear with the deflector position.

(3) No load flow characteristics

In Figure 10, when the load pressure decreases to zero, the load flow at this point is the no load flow between the two chambers. No load flow can reflect the response velocity of the pilot stage. The higher the no load flow is, the faster the response speed of the pilot stage is. It can be found from Figure 11 that with the increase of deflector position, no load flow increases gradually, but the flow gain gradually decreases.

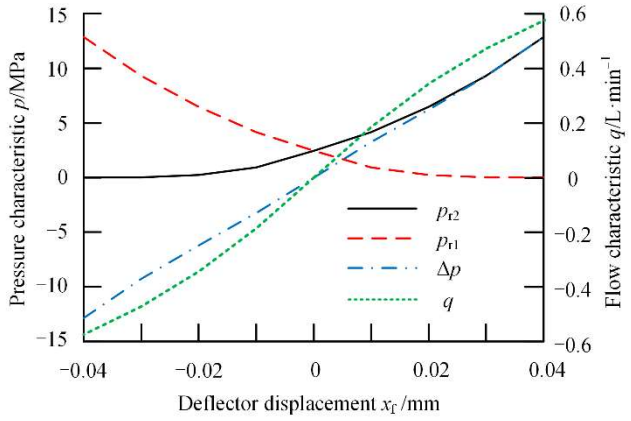

Figure 11 Pressure characteristics and flow characteristics of the pilot stage at different positions

4.2 Parameters' influence on static characteristics

In order to analyze the deflector structure parameters' influence on the zero-position characteristics, eight major parameters such as the width of jet nozzle a, the thickness of the jet-pan b, the length of receiving chamber L_r, the distance from jet nozzle to receiving chamber D, the thickness of the deflector d, the width of guide groove outlet a_n, the width of the wedge e and the half angle of guide groove θ are selected. Taking the data in Table 1 as the standard value D_{k0}, the structure parameters change from 0.8 standard value to 1.2 standard value.

When the above parameters are changed, the pressure-flow characteristics change as shown in Figure 12. It can be found that the influence of different parameters is significantly different. The increase of the width of jet nozzle a will cause the pressure-flow characteristics curve to move to the upper right and increase the cut-off load pressure and no-load flow at the same time; The thickness of the jet-pan b has a more obvious influence on the no-load flow, but it hardly changes the cut-off load pressure of the pilot stage; Contrary to the influence of parameter b, length of receiving chamber L_r have obvious influence on the cut-off load pressure, while the influence on the no-load flow is small; Increasing the width of guide groove outlet a_n and reducing the width of the wedge e can also increase cut-off load pressure significantly, as for the no-load flow, the increase of width of width of guide groove outlet will cause it increase first and then decrease, and the decrease of the width of the wedge will make it decrease first and then tend to be constant; Increasing the distance from jet nozzle to receiving chamber D or reducing the thickness of the deflector d will increase the cut-off load pressure but decrease the no-load flow; The half angle of guide groove θ has little influence on the pressure-flow characteristics.

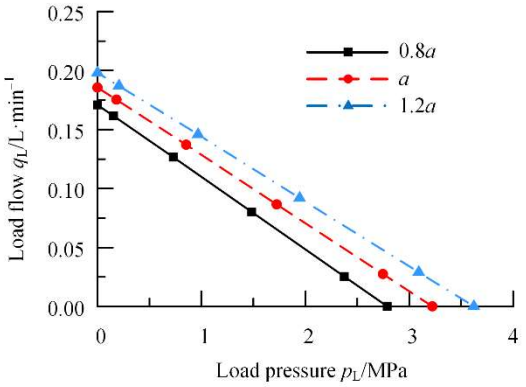

a) The width of jet nozzle a

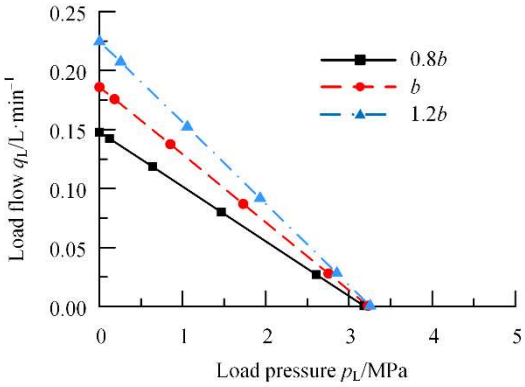

b) The width of jet nozzle b

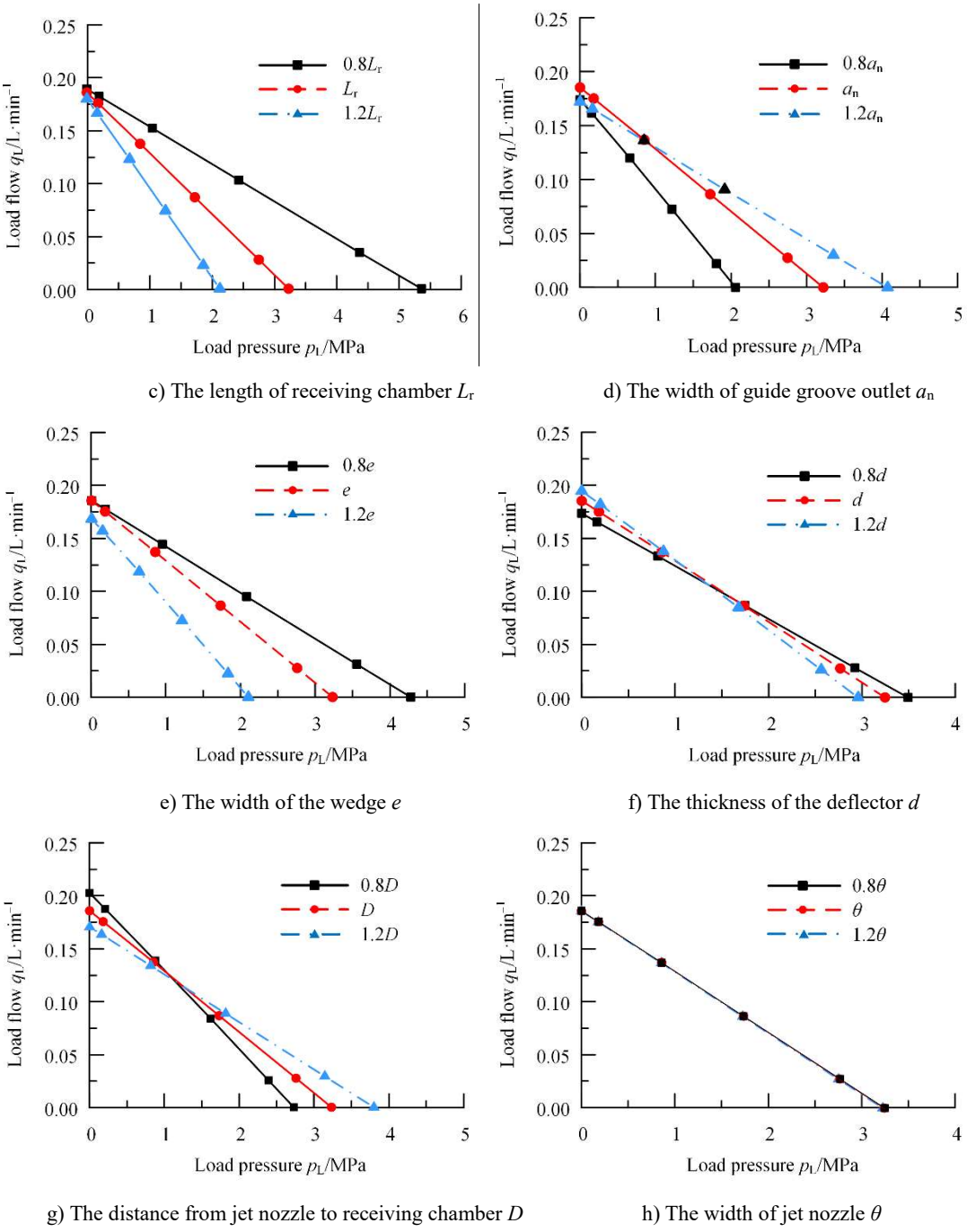

c) The length of receiving chamber L_r d) The width of guide groove outlet a_n

e) The width of the wedge e f) The thickness of the deflector d

g) The distance from jet nozzle to receiving chamber D h) The width of jet nozzle θ

Figure 12 Influence of different parameters on pressure-flow characteristics of the pilot stage

In the static characteristics of the servo valve, zero position characteristics are very important which include three valve coefficients. They are zero-position pressure gain k_{p0}, zero-position flow gain k_{q0} and flow-pressure coefficient k_{c0}. Figure 13a), b) and c) respectively show the influence of parameters on the valve coefficients. In order to facilitate the comparison of the relative influence of various structural parameters on the valve coefficient, the horizontal coordinate adopts the dimensionless form D_k/D_{k0}, and it can be clearly found through comparison:

(1) As shown in Figure 13a). Increasing the width of guide groove outlet a_n, the distance from jet nozzle to receiving chamber D, the width of jet nozzle a and reducing the length of receiving chamber L_r and the width of the wedge e and the thickness of the deflector d can improve the zero-position pressure gain. Among them, width of guide groove outlet a_n, length of receiving chamber L_r and width of the wedge e have the most obvious influence. The influence of the width

of the wedge e is more linear, the thickness of the jet-pan b and half angle of guide groove θ have little influence on pressure gain.

(2) As shown in Figure 13b). Increasing the width of jet nozzle a, the thickness of the jet-pan b, the distance from jet nozzle to receiving chamber D and reducing the thickness of the deflector d can improve the zero-position flow gain. the width of guide groove outlet a_n and the width of the wedge e have nonlinear influence on it. Increasing the width of guide groove outlet a_n will make flow gain increase first and then decrease. Reducing the width of the wedge e also increases the flow gain, but the flow gain tends to be saturated when the width of the wedge is small. The length of receiving chamber L_r and half angle of guide groove θ have smaller influence on the flow gain.

(3) The zero-position flow-pressure coefficient can be calculated by dividing the zero-position flow gain by the zero-position pressure gain. As shown in Figure 13c). Increasing the length of receiving chamber L_r, the width of the wedge e, the thickness of the jet-pan b, the thickness of the deflector d and reducing the distance from jet nozzle to receiving chamber D and the width of guide groove outlet a_n can improve the flow-pressure coefficient. Since Increasing the width of jet nozzle a will improve the cut-off load pressure and no load flow at the same time, the flow-pressure coefficient is basically unchanged. And the half angle of guide groove θ has little influence on cut-off load pressure and no load flow, so it has little influence on the flow-pressure coefficient too.

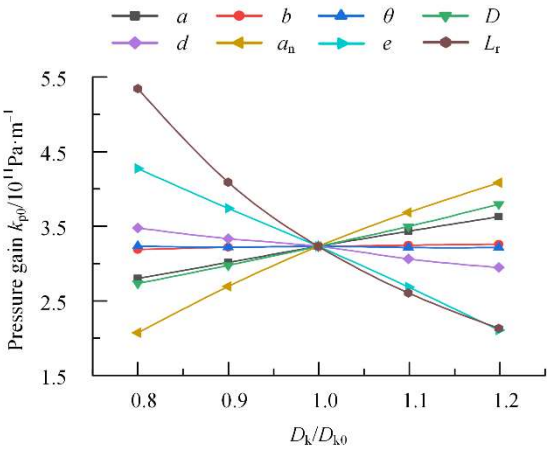

a) Zero-position pressure gain

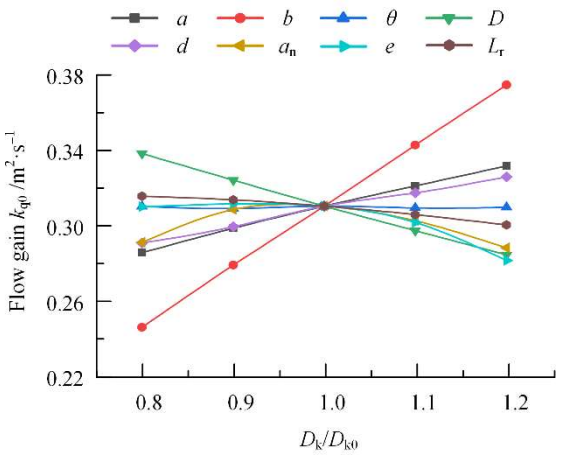

b) Zero-position flow gain

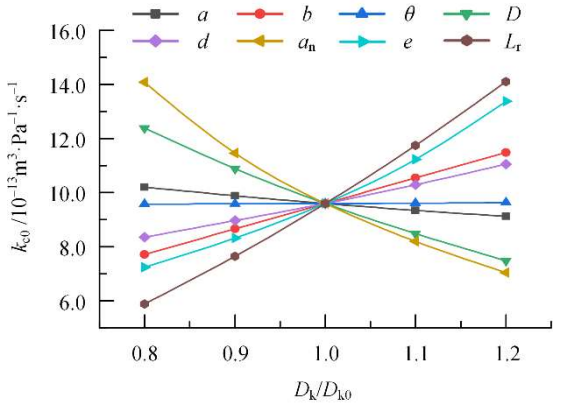

c) Zero-position flow-pressure coefficient

Figure 13 Structural parameters' influence on valve coefficients

The pilot stage with better static characteristics can be obtained through reasonable parameter optimization, but it is worth noting that the structure parameters also affect the other performance of the pilot stage. For example, the increase of width of jet nozzle and thickness of the jet-pan can also cause the increase of the leakage of pilot stage. Too low width of the wedge will not help increase the flow characteristics obviously, but it can aggravate the wedge wear instead. In addition, the deflector is much more difficult to process than the jet-pan, so the structural parameters optimization has to take the performance index requirements into consideration, targeted to carry on the design.

5 Numerical Study of Pilot Stage's Flow Field

The flow field of the pilot stage was studied through finite element simulation. The structural parameters are shown in Table 1. Different loads are simulated by thin-walled orifices

with diameters of 0.1 mm, 0.2 mm, 0.3 mm and 0.5 mm between the two receiving chambers. The supply pressure and return pressure of the flow field are set as 21 MPa and 0 MPa respectively. Aviation kerosene is used as transmission medium, k-ε turbulence model is selected for flow field model. The hexahedral mesh is used for mesh generation. The model with deflector displacement set as 0.01 mm and orifices diameter set as 0.1 mm is used for mesh independent verification. The verification result is shown in Table 2, when the number of nodes increases to more than 750,000, the simulation results of load pressure and load flow don't change significantly with the increase of the number of nodes. In order to balance the simulation time and solution accuracy, the number of nodes is set at about 850,000 for simulation, grid refinement is adopted in the core region of jet flow, the mesh generation result is shown in Figure 14.

Table 2 Grid nodes independent verification

Number of nodes	p_L/MPa	q_L/L·min^{-1}
545614	1.047	0.067
722194	1.742	0.096
852834	1.152	0.099
973364	1.175	0.097

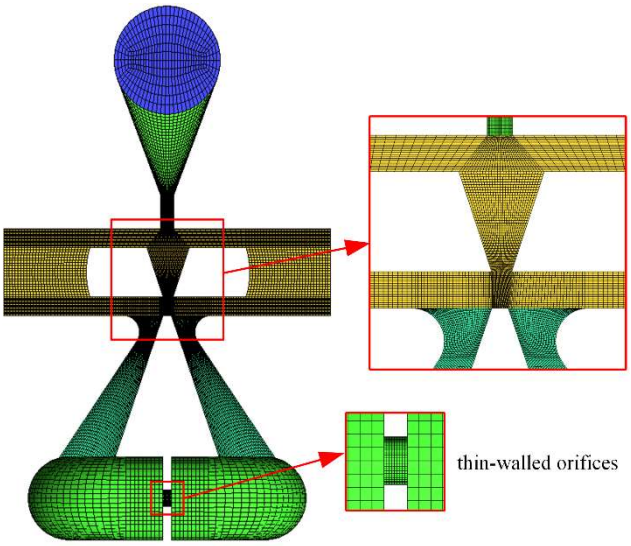

Figure 14 The result of the pilot stage meshing

5.1 Pressure-flow characteristics

Figure 15 a) and b) show the flow field velocity contour and pressure contour obtained by simulation. It can be found that the high-speed jet flow from the outlet of guide groove disperses at the wedge, due to the offset of the deflector. The flow into the right receiving chamber is more than that into the left receiving chamber, making the pressure of the right chamber higher than that of the left chamber. Driven by the pressure difference, part of the flow from the right receiving chamber flows into the left receiving chamber. The pressure at two points A and B in the figure is taken as the recovery pressure of the two chambers, and the pressure difference between the two points is taken as the load pressure. The load flow can be obtained by integrating the flow velocity through the orifices.

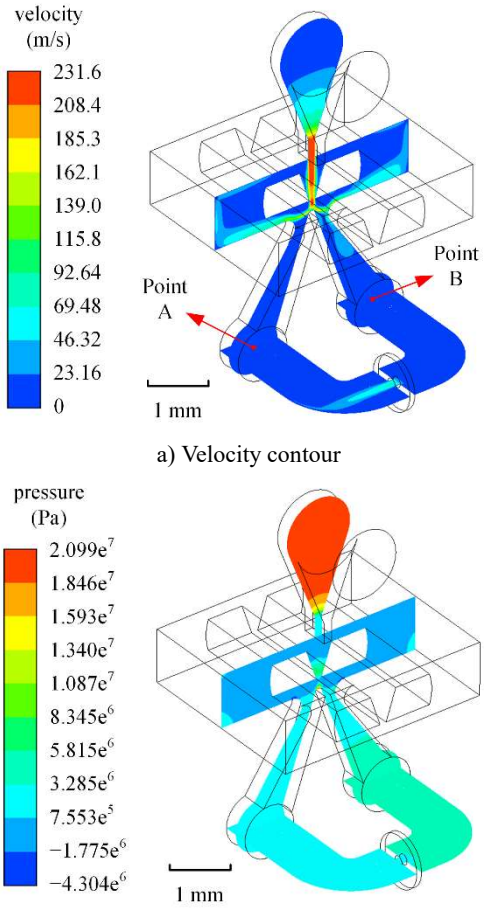

Figure 15 Simulation results of pilot stage's flow field

Figure 16 shows the finite element analysis results(Hereinafter referred to as the FEA result) of pressure-flow characteristics of the pilot stage under different deflector displacements. Compared with the model results(hereinafter referred to as the model result) based on the three dimensional flow field mentioned before, it can be found that the model result and the FEA result are in good agreement and the trend of pressure-flow characteristics curve is basically the same, but there are still some differences. The main difference is that the pressure-flow characteristics curve in the model result is approximately straight line. When the deflector position is fixed, the load flow decreases linearly with the load pressure. While the FEA result show that when the load pressure is less than four-fifths of the cut-off load pressure, there is a high

linearity between the load flow and the load pressure. The flow-pressure coefficient is basically the same as the model result. However, when the load pressure increases further, the load flow drops rapidly, resulting in a smaller cut-off load pressure than the model result.

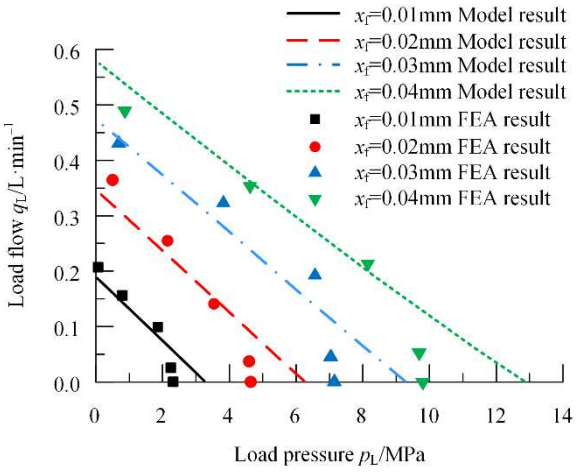

Figure 16 Pressure-flow characteristics of pilot stage compared between FEA result and model result

5.2 Three-dimensional jet in free jet region

Figure 17 is the velocity vector diagram of section 2-2 when the deflector is at zero position. It can be found that the jet expands in both the x direction and the y direction. In addition, the velocity distribution of the shear layer is approximate to the change rule of cosine function. In the yoz plane, the velocity in the middle of the flow field is slightly lower, while the velocity on both sides are slightly higher, which is similar to saddle shape. Furthermore, the velocity distribution in the streamwise direction at section 2-2 of deflector at zero and 0.04 mm is compared based on FEA result and model result, as shown in Figure 18. It is not difficult to find that the shape of the isovelocity line in the flow field is close to the shape of a straight slot, which is similar to the shape of the rectangular isovelocity line proposed in this paper. The higher the velocity is, the more obvious the rectangle feature of the isovelocity line is. With the offset of the deflector, the range of the constant velocity region expands, and the width of the shear layer decreases. These characteristics are consistent with the 3D turbulent jet model proposed in this paper, which confirms the rationality of the model in this paper.

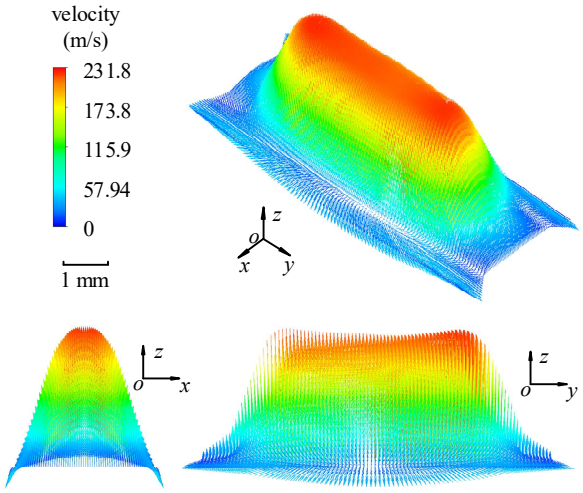

Figure 17 Velocity vector diagram of section 2-2 by FEA

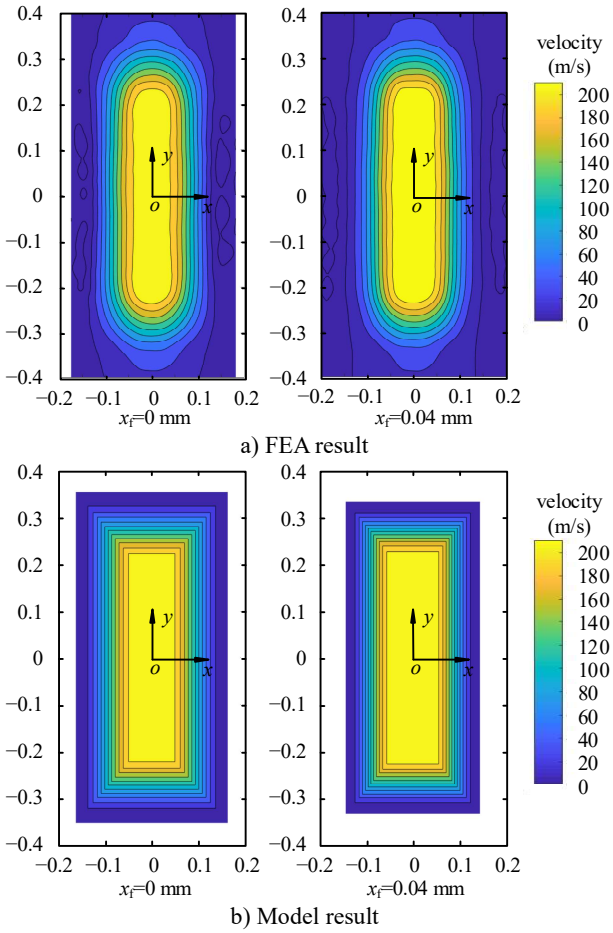

Figure 18 Velocity distribution along z direction at section 2-2

5.3 Jet entrainment in pressure recovery region

It can be found from Figure 19 that the secondary jet will still form entrainment due to mixing characteristics after entering the receiving chamber. As the flow field structure is symmetrical, the right receiving chamber is taken as an example for analysis.

In Figure 19a), the deflector position is 0.04 mm and the diameter of the damping orifice D_o is 0.5 mm and 0.1 mm respectively, the recovery pressure of the right receiving chamber is 2.74 MPa and 9.24 MPa respectively. It can be found that although the deflector position is same, the jet length is affected by the recovery pressure of the receiving chamber, the increase of pressure leads to the shortening of jet length and the reduction of entrainment flow.

Figure 19b) shows the flow field when the deflector position is 0.01 mm and 0.04 mm and the diameter of the damping orifice D_o is 0.5 mm. At this time, the recovery pressure of the right receiving chamber is 2.74 MPa and 2.22 MPa respectively. It can be found that although the recovery pressure is smaller when the deflector is at 0.01 mm, the jet length is shorter due to its smaller flow rate into the receiving hole at the 4-4 section. Therefore, the flow rate into the receiving chamber is another important factor related to entrainment flow rate.

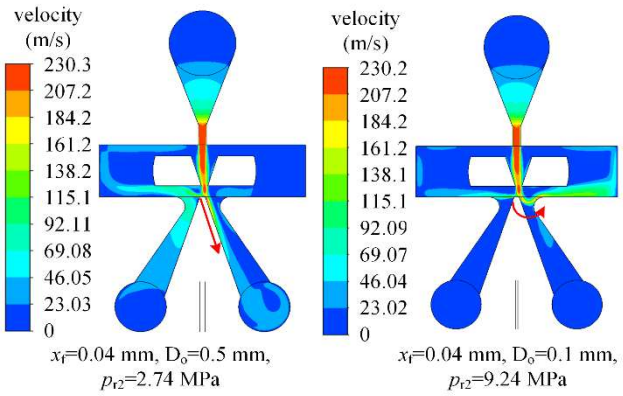

a) Velocity contour under different damping orifices

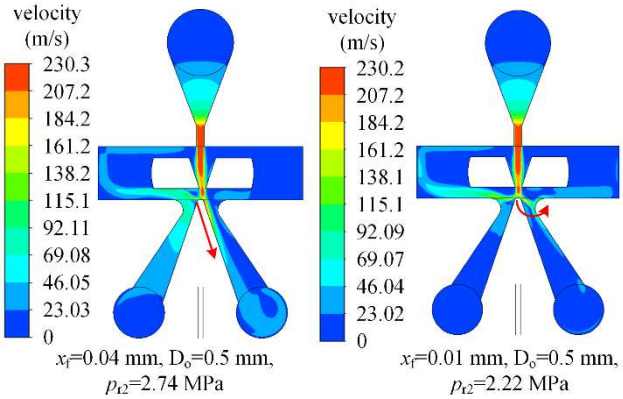

b) Velocity contour under different deflector positions

Figure 19　Jet entrainment in receiving chamber

In addition, jet entrainment is also related to the jet area when the deflector is at zero position. The jet entrainment makes the flow that enters the receiving chamber more, so ignoring jet entrainment will lead to lower recovery pressure of the receiving chamber. Therefore, in order to describe the coupling relationship between recovery pressure and jet flow and to get more accurate result, formula (23) is proposed to calculate the entrainment flow rate. It is a relatively simple expression. The precise calculation of entrainment flow rate is a very complex problem, which will be further studied in the future.

6　Experimental Verification

The pilot stage cut-off load pressure characteristics experiment of a DJSV is carried out on the test rig as shown in Figure 20 by Aviation Key Laboratory of Science and Technology on Aero Electromechanical System Integration, and the structure parameters of the pilot stage are consistent with those in Table 1. The medium is RP3 fuel, and the temperature is 17℃~20℃. The return pressure is 0, the oil supply pressure p_s is 1 MPa, 5 MPa and 10 MPa respectively. Figure 21 shows the experimental principle, an extension board is attached to the armature facilitate the measurement of the armature displacement. The armature displacement is measured by the laser displacement sensor(KEYENCE LK-H025 Series, whose measurement resolution is 0.01 μm), and then the deflector displacement is obtained by indirect calculation. The recovery pressure is measured by the pressure gauge. Due to the inevitable errors in the installation of the deflector, null bias exists in the pilot stage. When the deflector displacement is 0, the cut-off load pressure is not 0, and the null bias changes with the supply pressure(known as supply pressure null shift). In order to avoid the influence of null bias, it is necessary to correct the deflector displacement by subtracting the measured value plus the null bias value which means the deflector displacement when the cut-off load pressure is 0. By measurement, the null bias value under 1 MPa,5 MPa and 10 MPa are −1.8 μm, 0 μm and 6.3 μm respectively. Experimental data under different oil supply pressures are shown in Table 3

Table 3 Cut-off load pressure under different oil supply pressures

a) Cut-off load pressure experimental data when p_s=1 MPa

Measured deflector displacement(μm)	Deflector displacement after correction(μm)	Cut-off load pressure(MPa)
0.00	1.80	0.04
6.29	8.09	0.14
13.52	15.32	0.26
20.09	21.89	0.35
30.87	32.67	0.45
42.54	44.34	0.53

b) Cut-off load pressure experimental data when p_s=5 MPa

Measured deflector displacement(μm)	Deflector displacement after correction(μm)	Cut-off load pressure(MPa)
3.49	3.49	0.32
17.14	17.14	1.48
33.27	33.27	2.7
43.67	43.67	3.18

c) Cut-off load pressure experimental data when p_s=10 MPa

Measured deflector displacement(μm)	Deflector displacement after correction(μm)	Cut-off load pressure(MPa)
7.84	1.54	0.3
10.95	4.65	0.82
14.11	7.81	1.31
18.00	11.70	1.96
20.99	14.69	2.41

Figure 22 shows the comparison of the model results with the experimental results for dimensionless cut-off load pressure characteristics. It can be found from experimental data that when the deflector displacement is small, the dimensionless pressure under different oil supply pressures are close to each other, while when the deflector displacement is large, the increase of oil supply pressure makes the dimensionless pressure increase, and the model calculation also shows that there is little difference in the dimensionless pressure characteristics under different supply pressures. The model results are in good agreement with the experimental results, which indicates the reliability of the mathematical model of the pilot stage.

a) Pilot stage pressure characteristics test rig

b) Photograph of jet-pan

Figure 20 Experimental setup

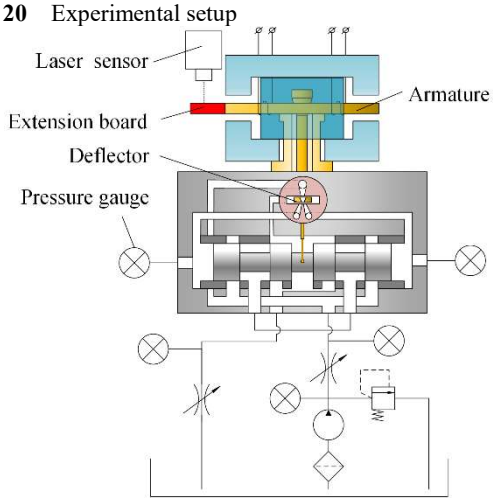

Figure 21 Schematic diagram of experimental set-up

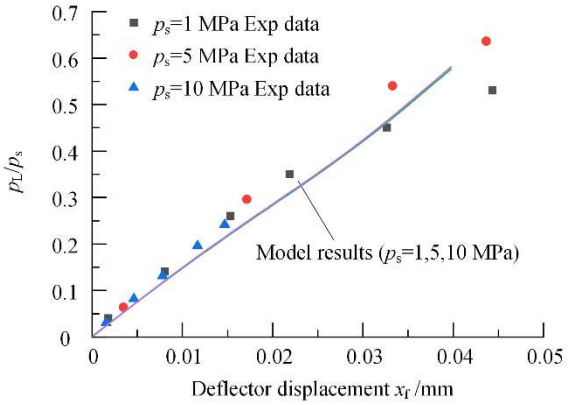

Figure 22 Dimensional cut-off load pressure characteristics

7 Conclusions

(1) The three-dimensional flow law of the pilot stage's flow field of the DJSV is revealed, and the coupling relationship between the pressure of the receiving chamber and the jet flow is found out. A new flow field model for the pilot stage of the DJSV is established. In particular, 3D jet model is proposed in the free jet region, and jet entrainment model is proposed in the pressure recovery region for the first time. The static characteristics calculated by the flow field model established is in line with the result obtained by FEA, the correctness of the 3D jet model and the jet

expansion model is further verified. And the result of the dimensionless cut-off load pressure characteristics is in good agreement with the experimental result.

(2) The pressure-flow characteristics, pressure characteristics and flow characteristics of the pilot stage under different deflector displacements are derived. The main structural parameters that affect the zero-position pressure gain include the length of receiving chamber, the width of guide groove outlet and the width of the wedge, but the thickness of the jet-pan has little influence on zero-position pressure gain. The main structural parameters that affect the zero-position flow gain include the width of jet nozzle and the thickness of the jet-pan, the width of guide groove outlet and the width of the wedge have nonlinear influence on zero-position flow gain. The pilot stage with better static characteristics can be obtained through reasonable parameter optimization.

8 Declaration

Funding

Supported by National Natural Science Foundation of China (Grant No. 51775383)

Availability of data and materials

The datasets supporting the conclusions of this article are included within the article.

Authors' contributions

The author's contributions are as follows: Yao-Bao Yin was in charge of the whole trial; Shuang-Lu Li wrote the manuscript; Jia-Yang Yuan and Sheng-Rong Guo assisted with laboratory analyses.

Competing interests

The authors declare no competing financial interests.

Consent for publication

Not applicable

Ethics approval and consent to participate

Not applicable

References

[1] R H Maskrey, W J Thayer. A brief history of electrohydraulic servomechanisms. *Journal of Dynamic Systems Measurement & Control*, 1978, 100(2):110.

[2] P Tamburrano, A R Plummer, E Distaso, et al. A review of electro-hydraulic servovalve research and development. *International Journal of Fluid Power*, 2018: 1-23.

[3] S H Somashekhar, M Singaperumal, R K Kumar. Modelling the steady-state analysis of a jet pipe electrohydraulic servo valve. *Proceedings of the Institution of Mechanical Engineers, Part I: Journal of Systems and Control Engineering*, 2006, 220(2): 109-129.

[4] Y S Liu, J Dong, S Wu, et al. Theoretical research on the dynamic characteristics of electrohydraulic servo valve(EHSV) in deep sea environment. *Ocean Engineering*, 2019, 192: 105957.1-105957.12.

[5] J Yu, J Zhuang, D H Yu. Modeling and Analysis of A Rotary Direct Drive Servovalve. *Chinese Journal of Mechanical Engineering*, 2014, 27(5): 1064-1074.

[6] Y B Yin, J Y Yuan, S R Guo. Numerical study of solid particle erosion in hydraulic spool valves. *Wear*, 2017, 392: 174-189.

[7] D R Gao, H J Qiao, X H Lu. Finite element numerical simulation and PIV measurement of flow field inside metering-in spool valve. *Chinese Journal of Mechanical Engineering*, 2009, 23(1).

[8] S J Li, N Z Aung, S Z Zhang, et al. Experimental and numerical investigation of cavitation phenomenon in flapper–nozzle pilot stage of an electrohydraulic servo-valve. *Computers & fluids*, 2013, 88: 590-598.

[9] P Tamburrano, A R Plummer, P D Palma, et al. A novel servovalve pilot stage actuated by a piezo-electric ring bender: A numerical and experimental analysis. *Energies*, 2020, 13(3): 671.

[10] T Alfred. *Regulating device including a distributor having double-acting knife-edges*: U.S. Patent 3,223,103. 1965-12-14.

[11] E F Mcfadden, L J Williams. *Free jet stream deflector servovalve*: U.S. Patent 3,542,051. 1970-11-24.

[12] Y B Yin, P Zhang, B Cen. Pre-stage flow field analysis on defector jet servo valves. *Chinese Journal of Construction Machinery*, 2015, 13(1): 1-7. (in Chinese)

[13] Y S Li. Mathematical modelling and characteristics of the pilot valve applied to a jet-pipe/deflector-jet servovalve. *Sensors & Actuators A Physical*, 2016, 245: 150-159.

[14] X L Ma. Model and simulation for deflector jet electrohydraulic servovalve. *Chinese Hydraulics & Pneumatics*, 2015, (3): 83-85, 89. (in Chinese)

[15] B K Saha, S J Li, X B Lv. Analysis of pressure characteristics under laminar and turbulent flow states inside the pilot stage of a deflection flapper servo-valve: Mathematical modeling with CFD study and experimental validation. *Chinese Journal of Aeronautics*, 2020, 33(3): 1107-1118.

[16] H Yan, Y K Ren, L Yao. et al. Analysis of the internal characteristics of a deflector jet servo valve. *Chinese Journal of Mechanical Engineering*, 2019, 32(1): 31.

[17] Y B Yin, S L Li, X W Zhang, et al, Steady-state flow force calculation of the first stage in a deflector jet servo valve. *2019 IEEE 8th International Conference on Fluid Power and Mechatronics* (FPM), Wuhan, China, April 10-13, 2019: 452-458.

[18] H Yan, S Kang, J Song, et al, Research on the calculation methods of flow force at pilot stage of jet deflector servo valve based on the simulated discrete data. *Journal of Mechanical Engineering*, 2016, 52(12): 181-191. (in Chinese)

[19] B K Saha, J H Peng, S J Li. Numerical and experimental investigations of cavitation phenomena inside the pilot stage of the deflector jet Servo-Valve. *IEEE Access*, 2020, 8: 64238-64249.

[20] D K Sangiah, A R Plummer, C R Bowen, et al. A novel piezohydraulic aerospace servovalve. Part 1: design and modelling. *Proceedings of the Institution of Mechanical Engineers, Part I: Journal of Systems and Control Engineering*, 2013, 227(4): 371-389.

[21] Y S Li, Y C Zhu, H T Wu, et al. Parameter optimization of jet-pipe servovalve driven by giant magnetostrictive actuator. *Acta*

Aeronautica et Astronautica Sinica, 2011, 32(7): 1336-1344. (in Chinese)

[22]Y Y Sheng, P J Zhang, S L Nie. Energy loss of nozzles in water jet system. *Journal of Mechanical Engineering*,2013,49(02):139-145. (in Chinese)

[23]N Rajaratnam. *Turbulent jets*. Elsevier, 1976.

[24]P M Sforza, M H Steiger, N Trentacoste. Studies on three-dimensional viscous jets. *AIAA journal*, 1966, 4(5): 800-806.

[25]G F Marsters. Spanwise velocity distributions in jets from rectangular slots. *AIAA Journal*, 1981, 19(2): 148-152.

[26]H B Squire, Trouncer J. Round jets in a general stream. Reports and memoranda no. 1974, *Aeronautical Research Committee*, London; 1944.

Biographical notes

Shuang-Lu Li, born in 1995, is currently a PhD candidate at *School of Mechanical Engineering, Tongji University, China*. He received his bachelor degree from *Yanshan University, China*, in 2017. His research interests include electro-hydraulic servo components.
Tel: +86-185-1218-3901; E-mail: 1710765@tongji.edu.cn

Yao-Bao Yin, born in 1965, is currently a professor at *Tongji University, China*. He received his PhD degree from *Saitama Universtiy, Japan,* in 1999. His research interests include electro-hydraulic servo system and components.
Tel: +86-137-7431-3727; E-mail: y-yin@tongji.edu.cn

Jia-Yang Yuan, born in 1992, is currently an engineer at *Nanjing Mechatronic and Hydraulic Engineering Research Centre* and *Aviation Key Laboratory of Science and Technology on Aero Electromechanical System Integration, China*.
E-mail: jiayangyuan2010@163.com

Sheng-Rong Guo, born in 1963, is currently a research fellow at *Nanjing Mechatronic and Hydraulic Engineering Research Centre* and *Aviation Key Laboratory of Science and Technology on Aero Electromechanical System Integration, China*.
E-mail: guosr@126.com

Figures

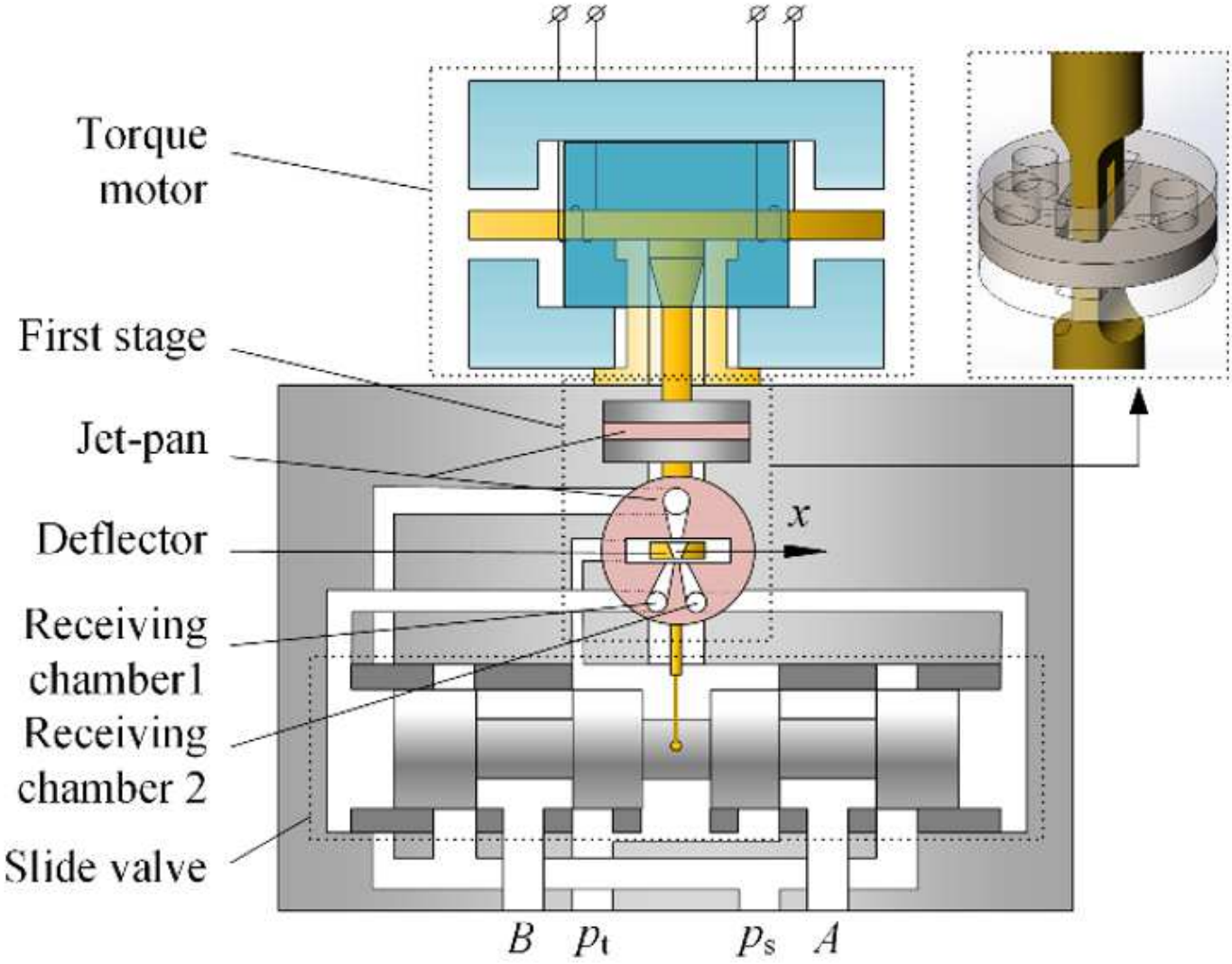

Figure 1

Working principle of the DJSV

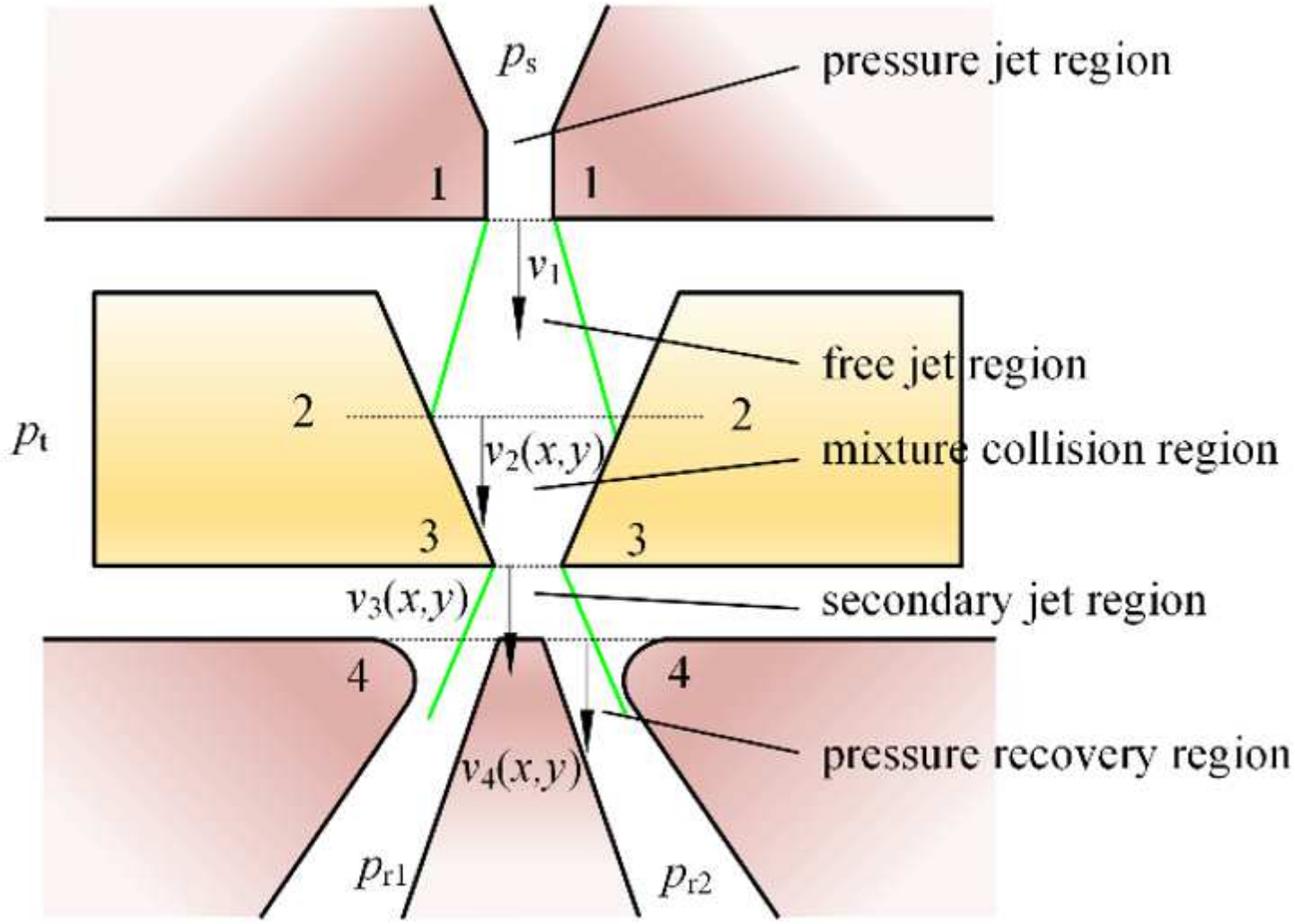

Figure 2

Flow field partition diagram

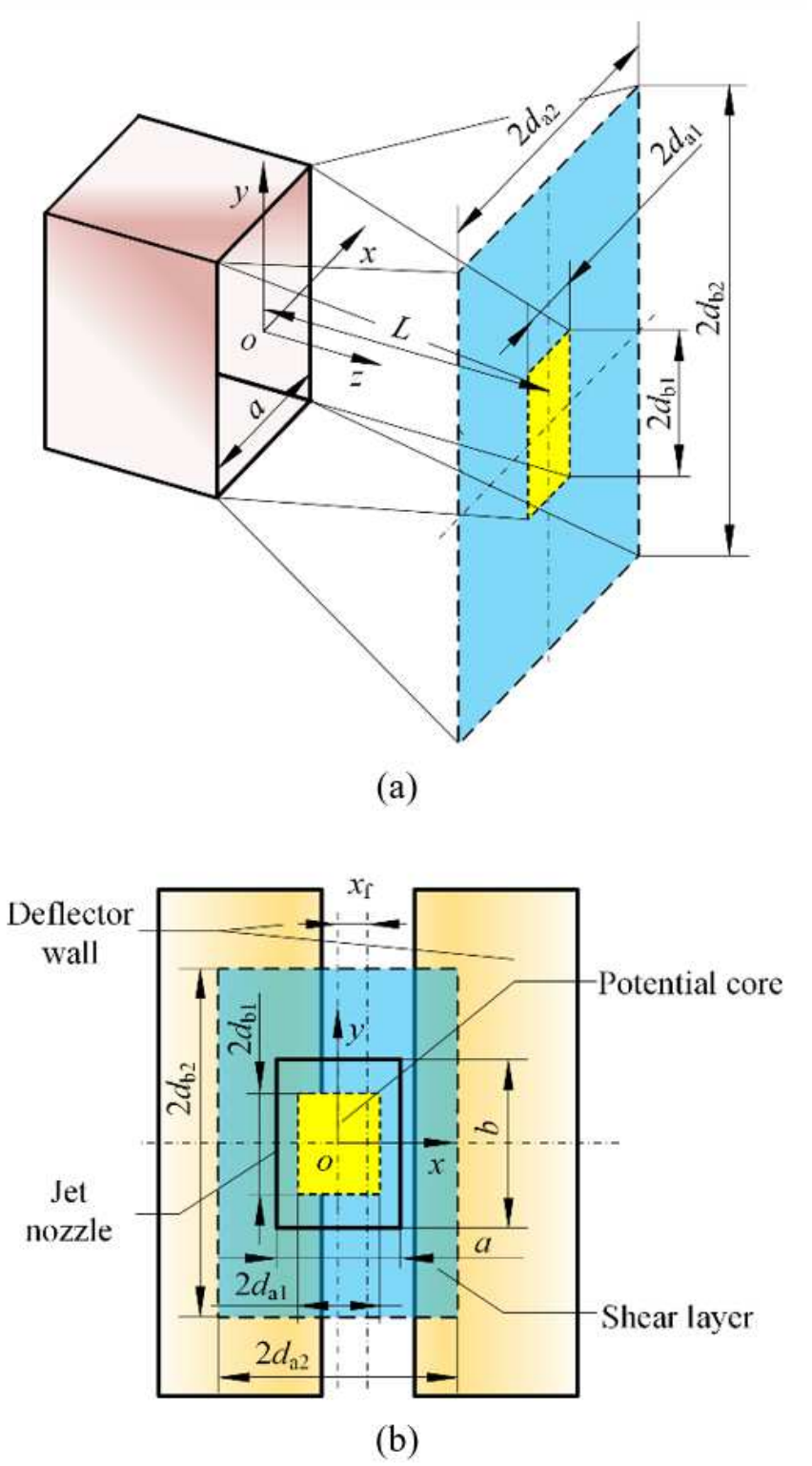

Figure 3

Schematic diagram of the free jet region

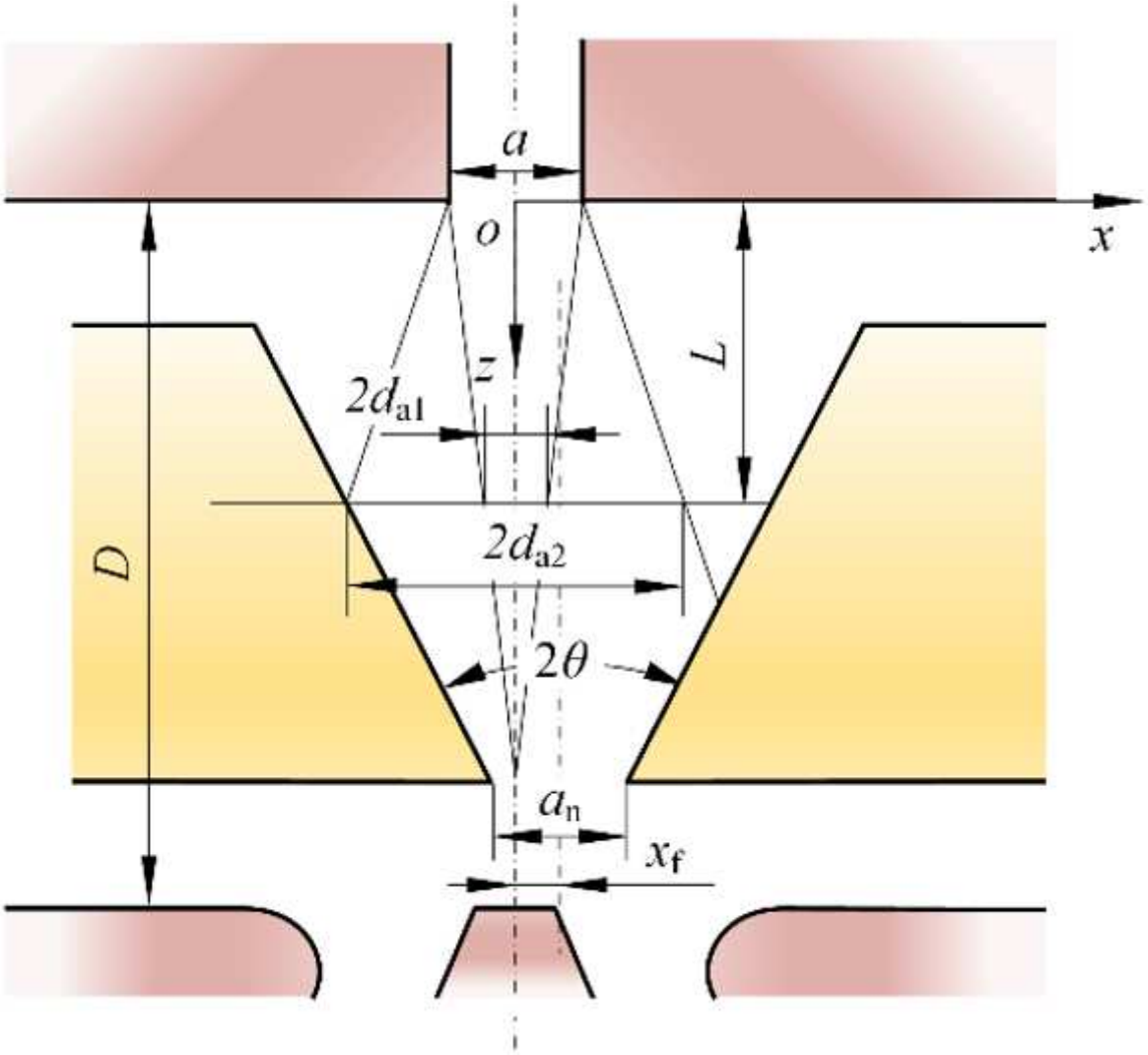

Figure 4

Structural parameters of the jet and the pilot stage

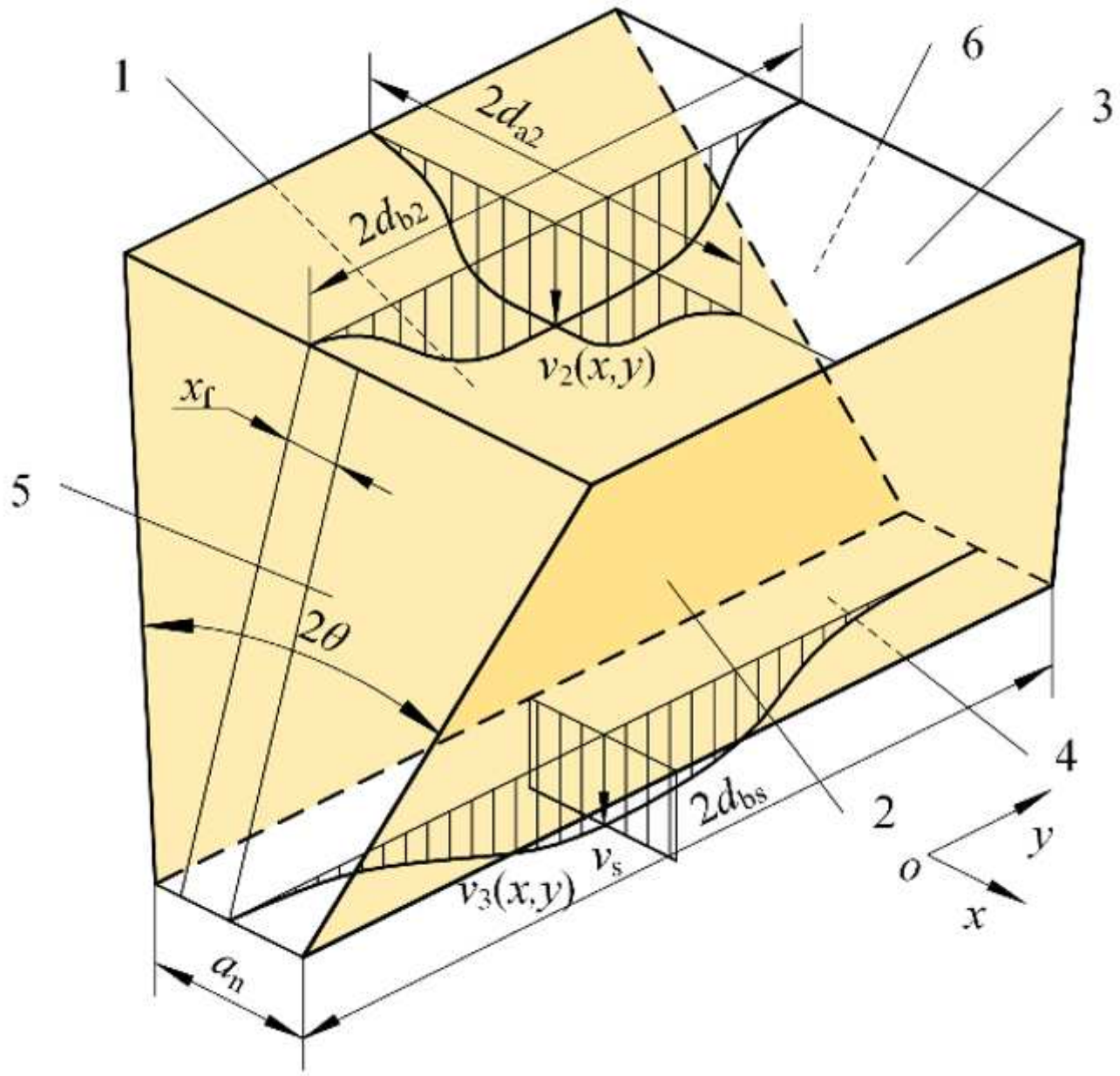

Figure 5

Schematic diagram of mixed jet region

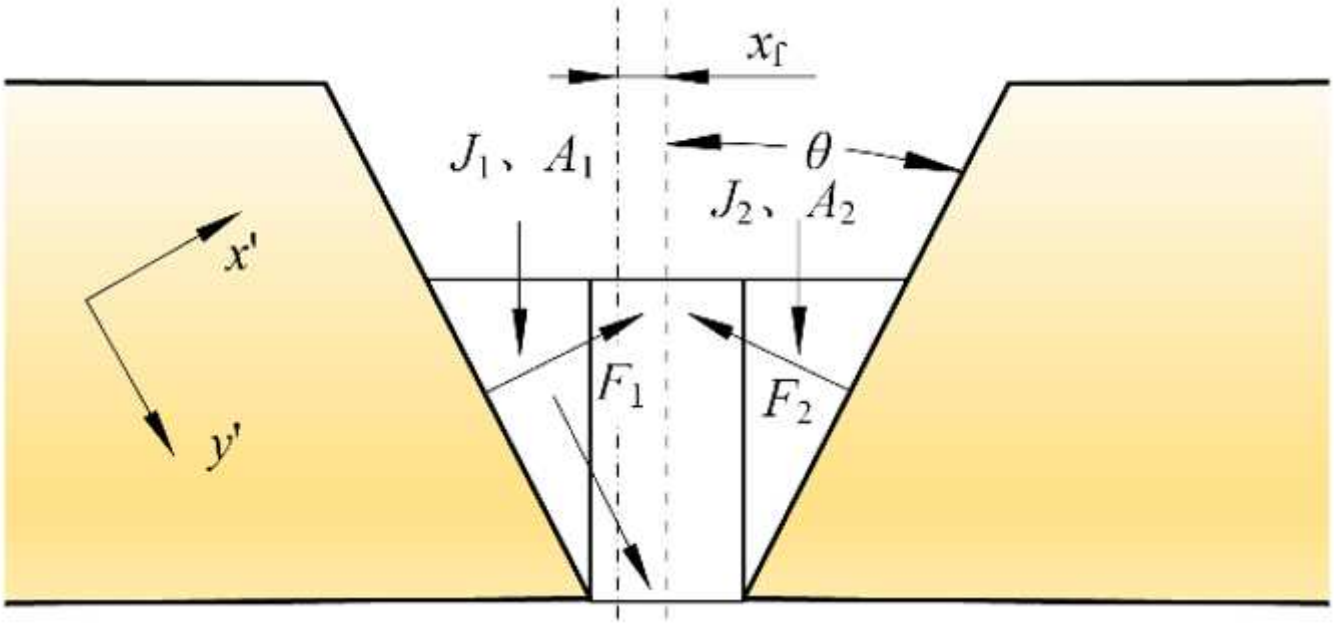

Figure 6

Schematic diagram of mixed jet region

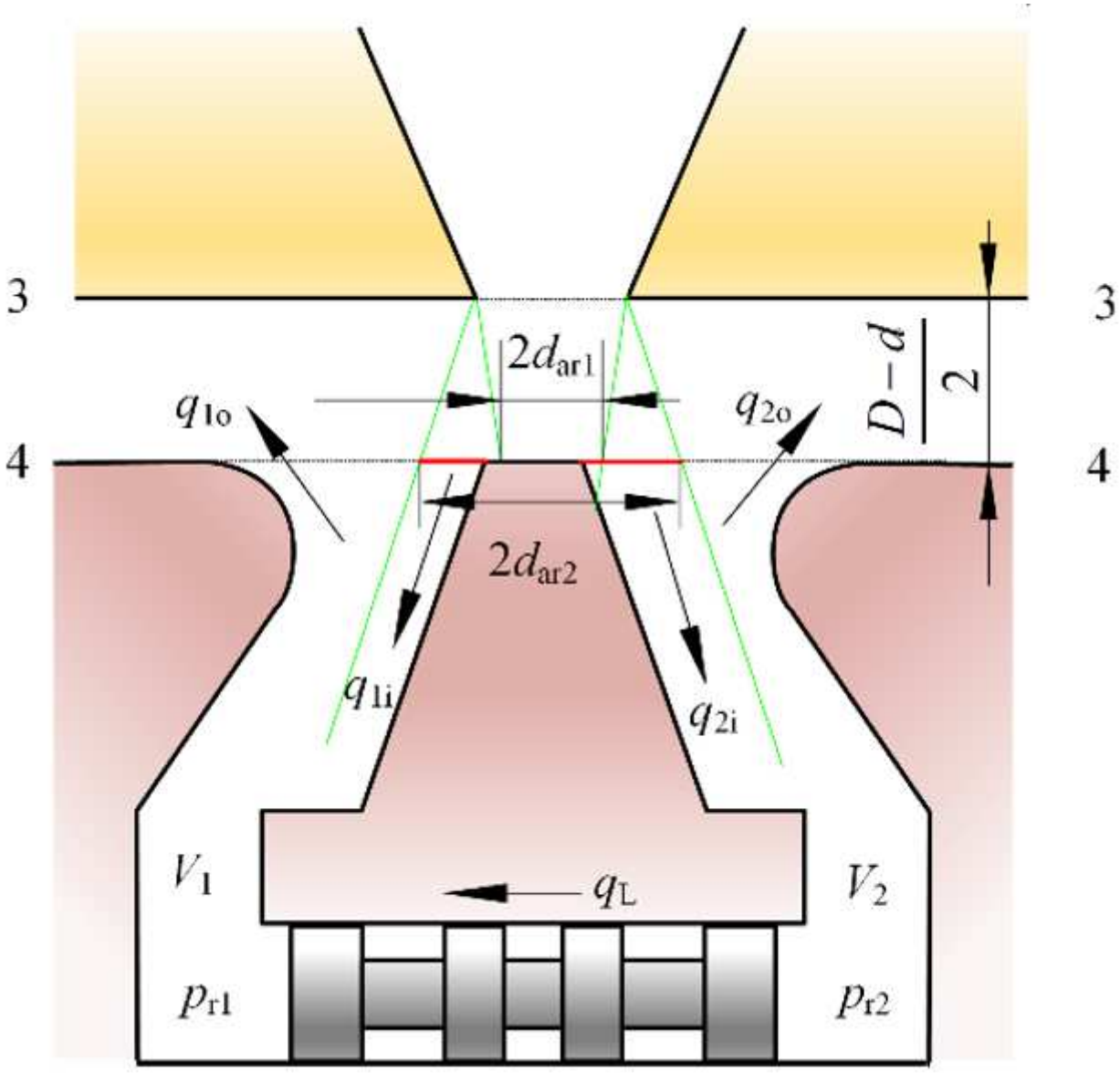

Figure 7

Schematic diagram of secondary jet region and pressure recovery region

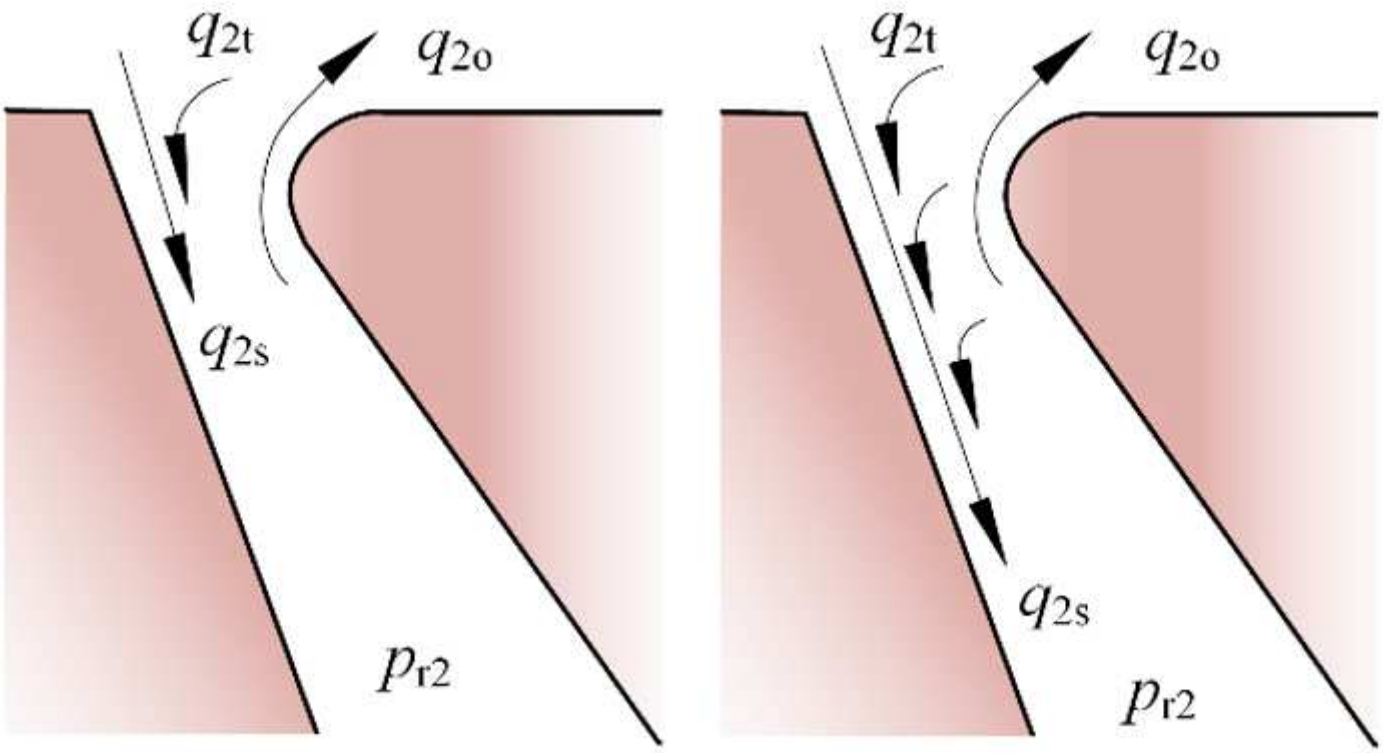

Figure 8

Schematic diagram of jet entrainment

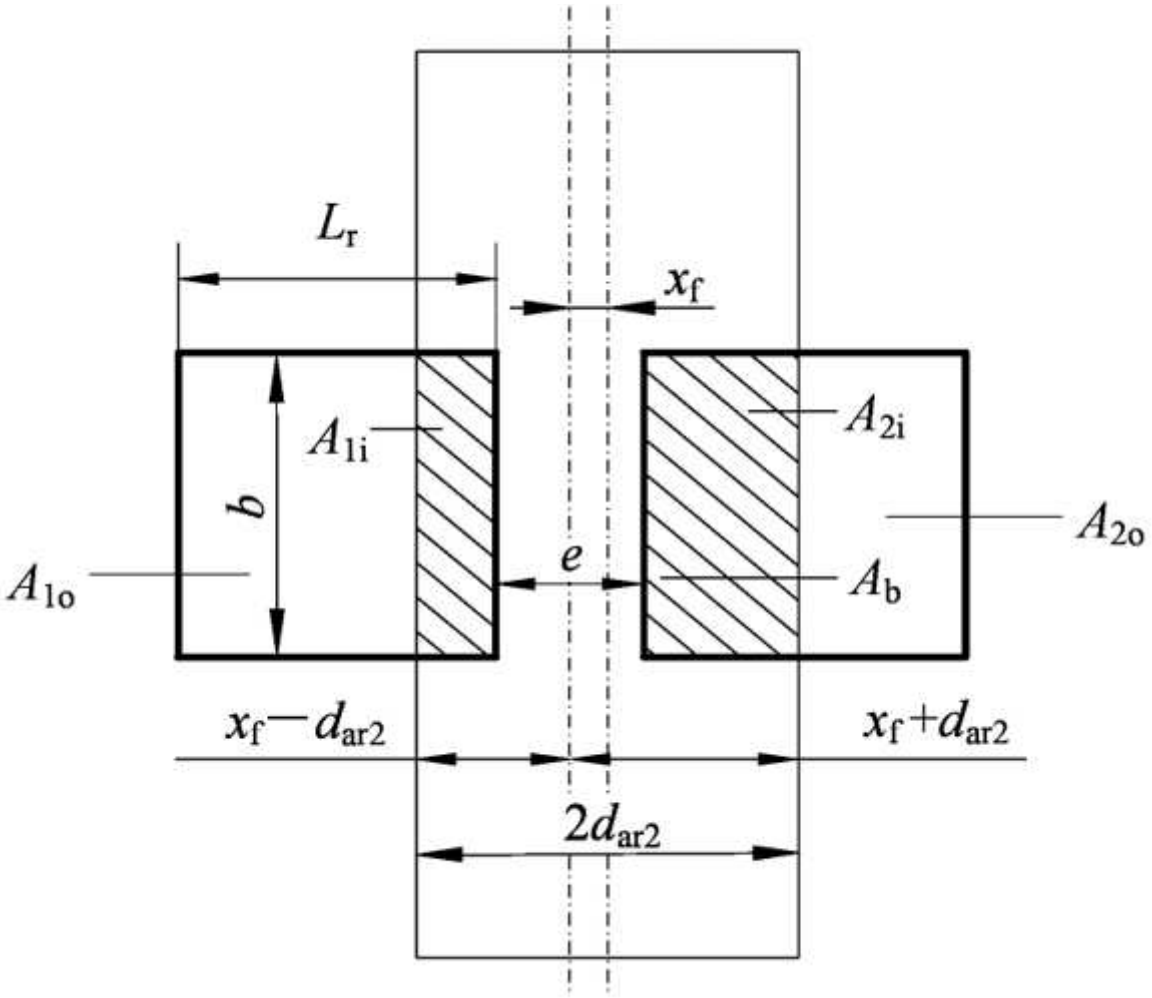

Figure 9

Structure diagram of receiving area

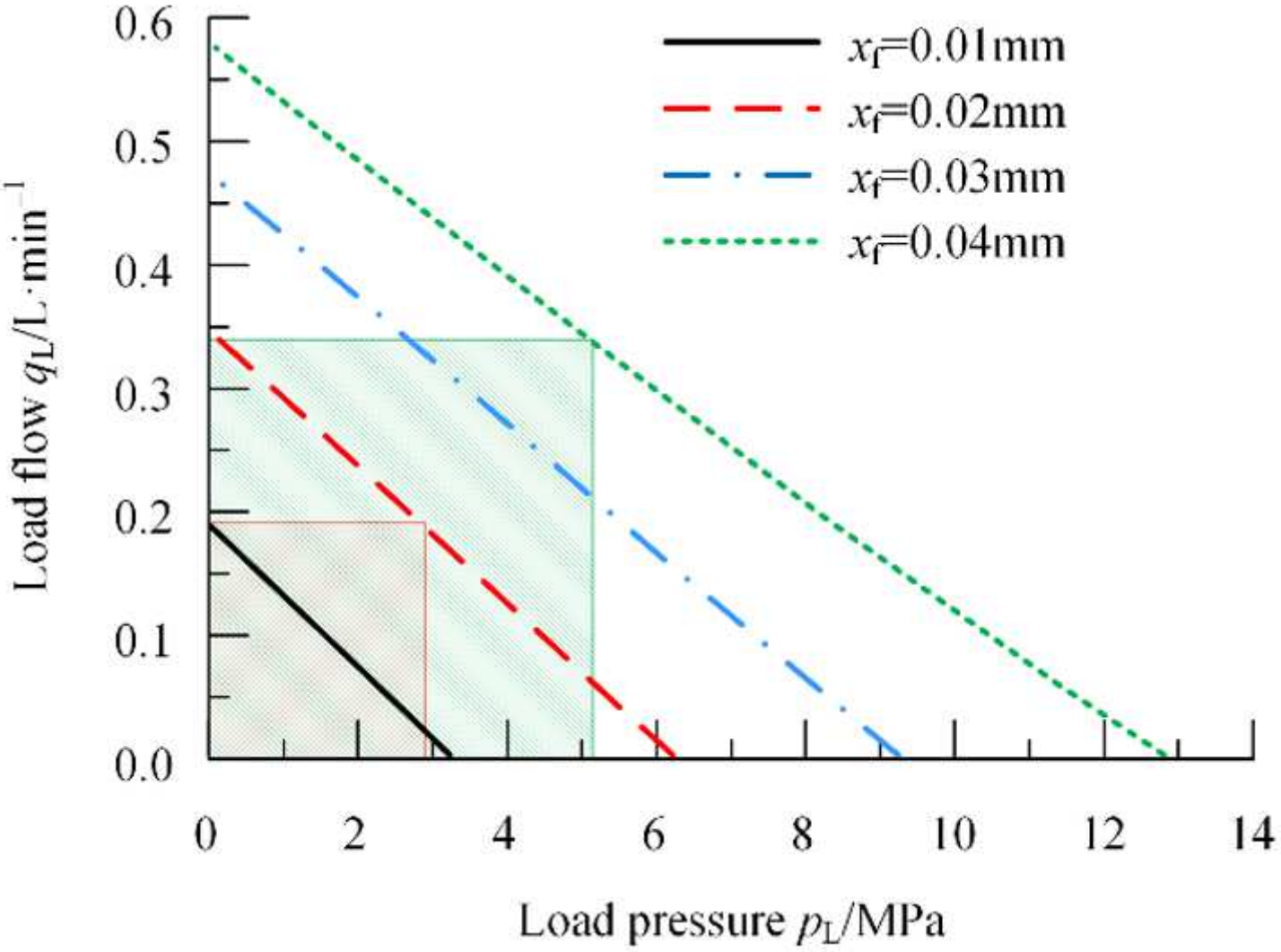

Figure 10

Pressure-flow characteristics of the pilot stage at different positions

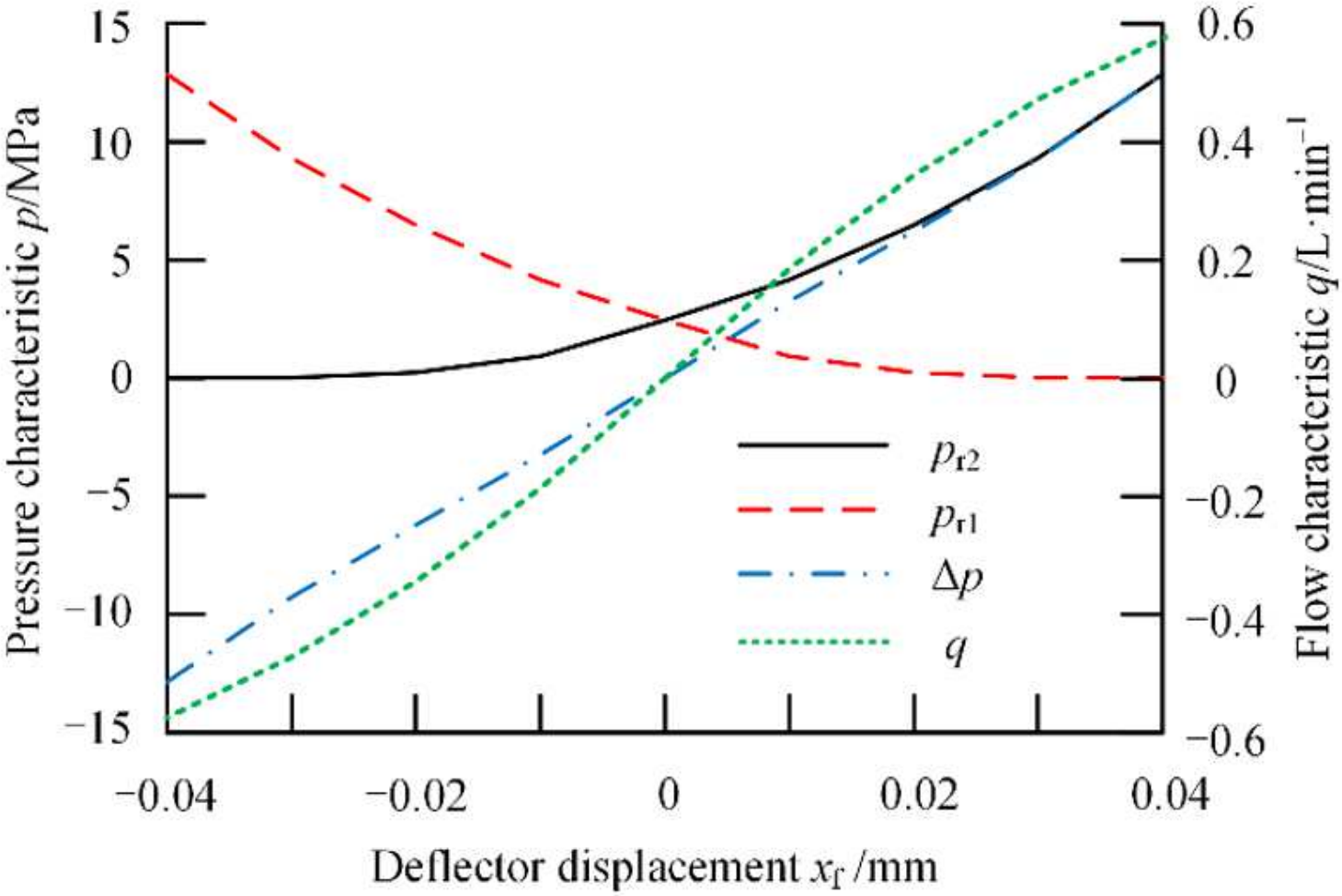

Figure 11

Pressure characteristics and flow characteristics of the pilot stage at different positions

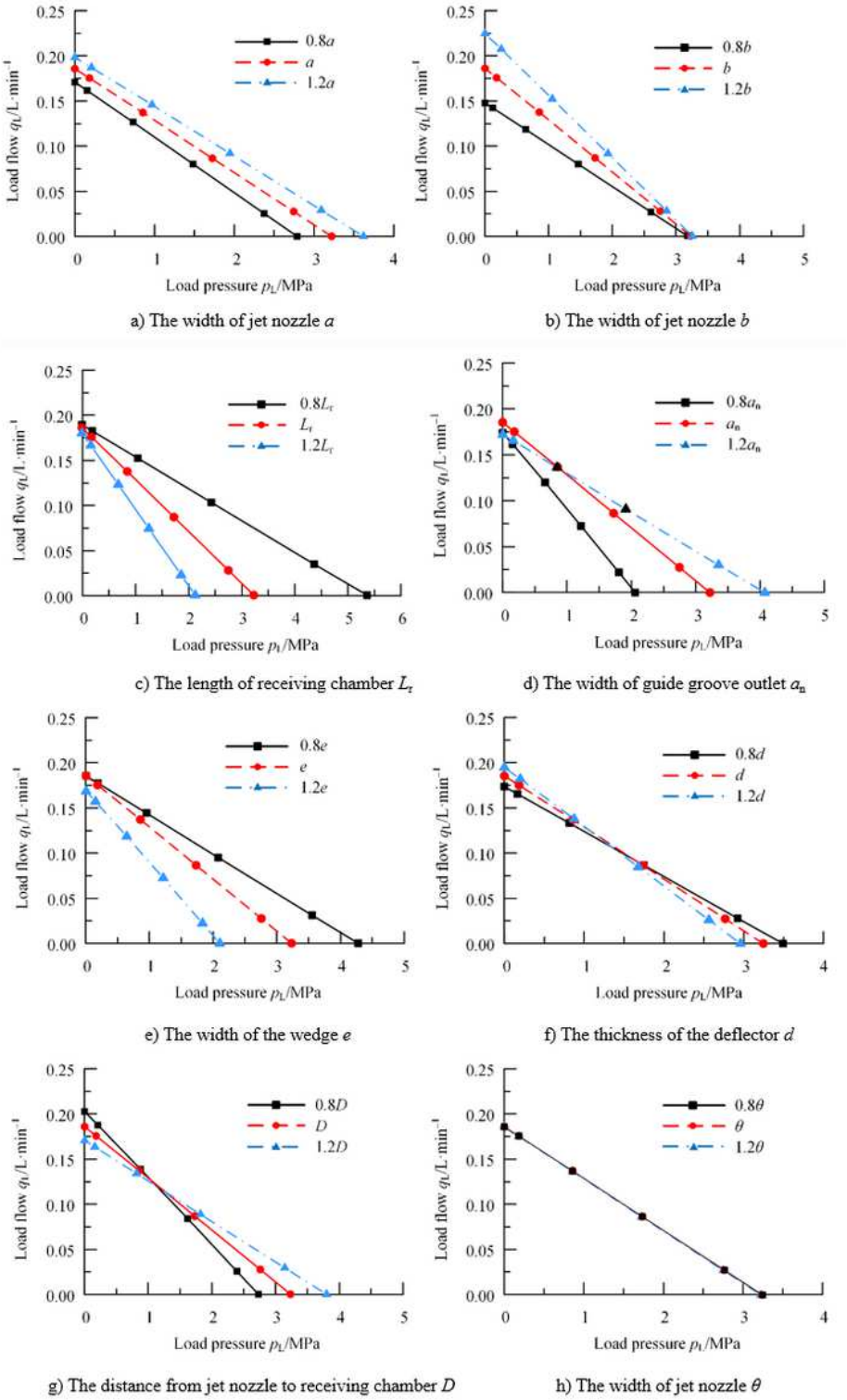

Figure 12

Influence of different parameters on pressure-flow characteristics of the pilot stage

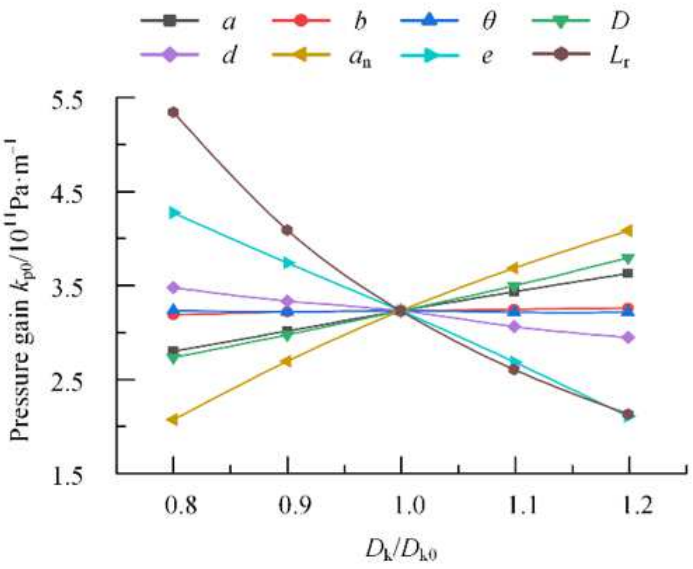

a) Zero-position pressure gain

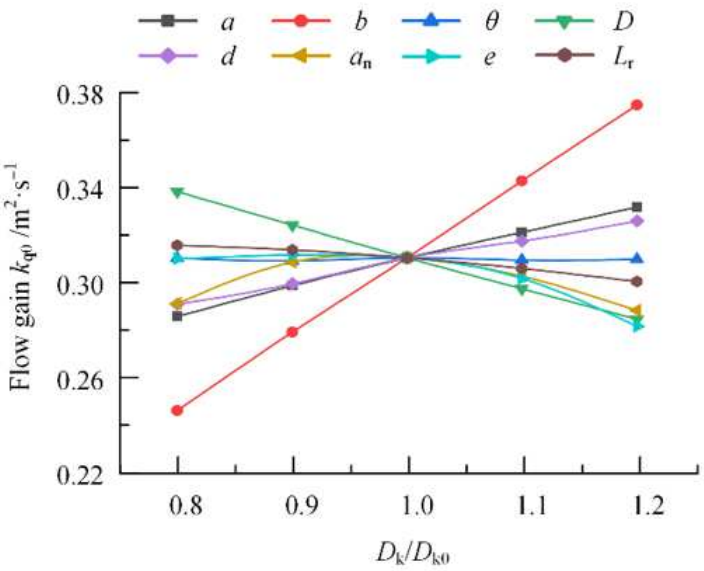

b) Zero-position flow gain

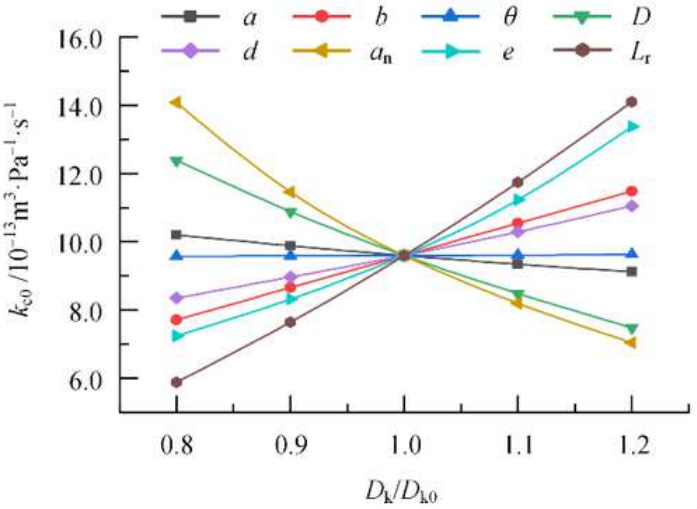

c) Zero-position flow-pressure coefficient

Figure 13

Structural parameters' influence on valve coefficients

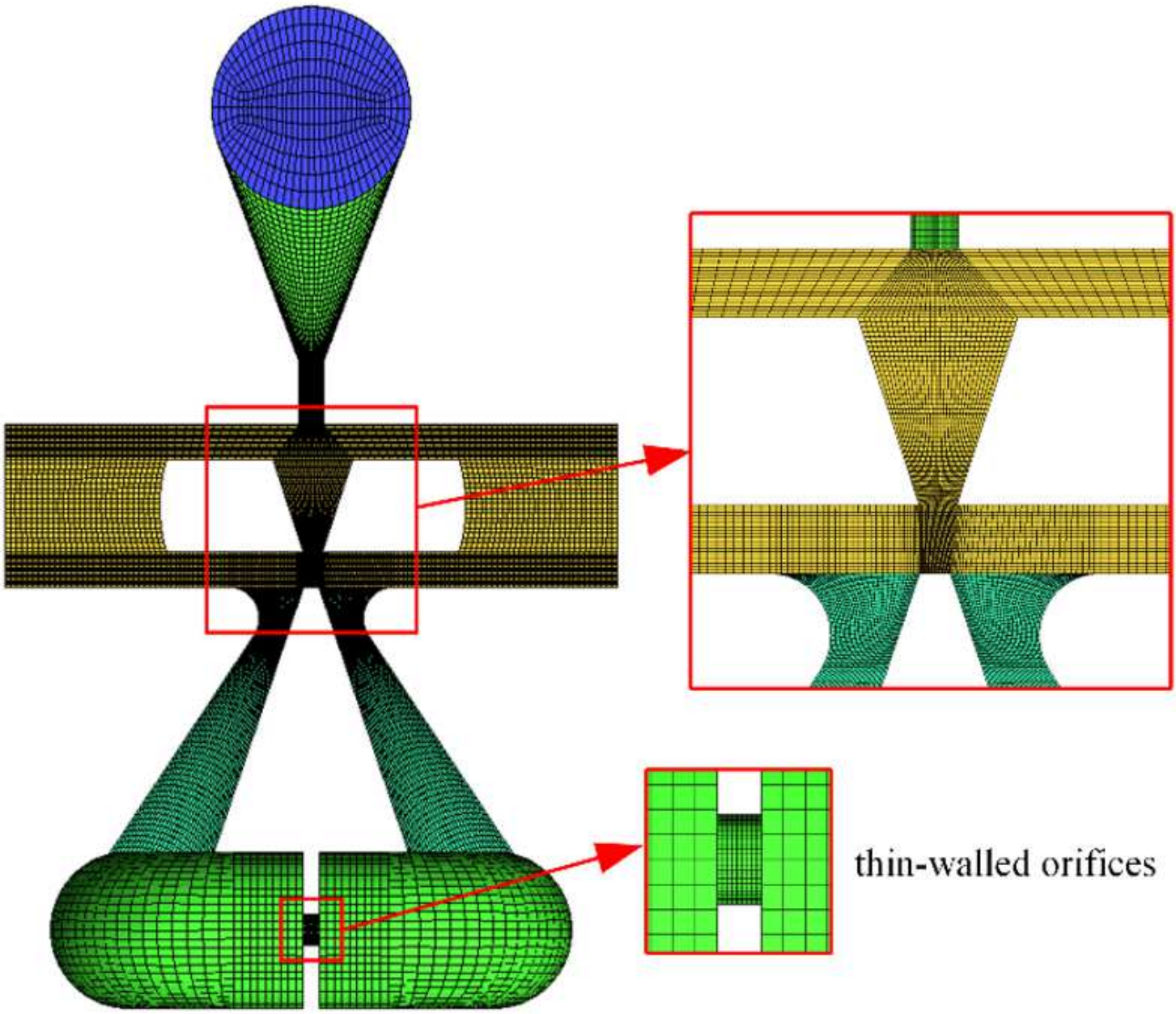

Figure 14

The result of the pilot stage meshing

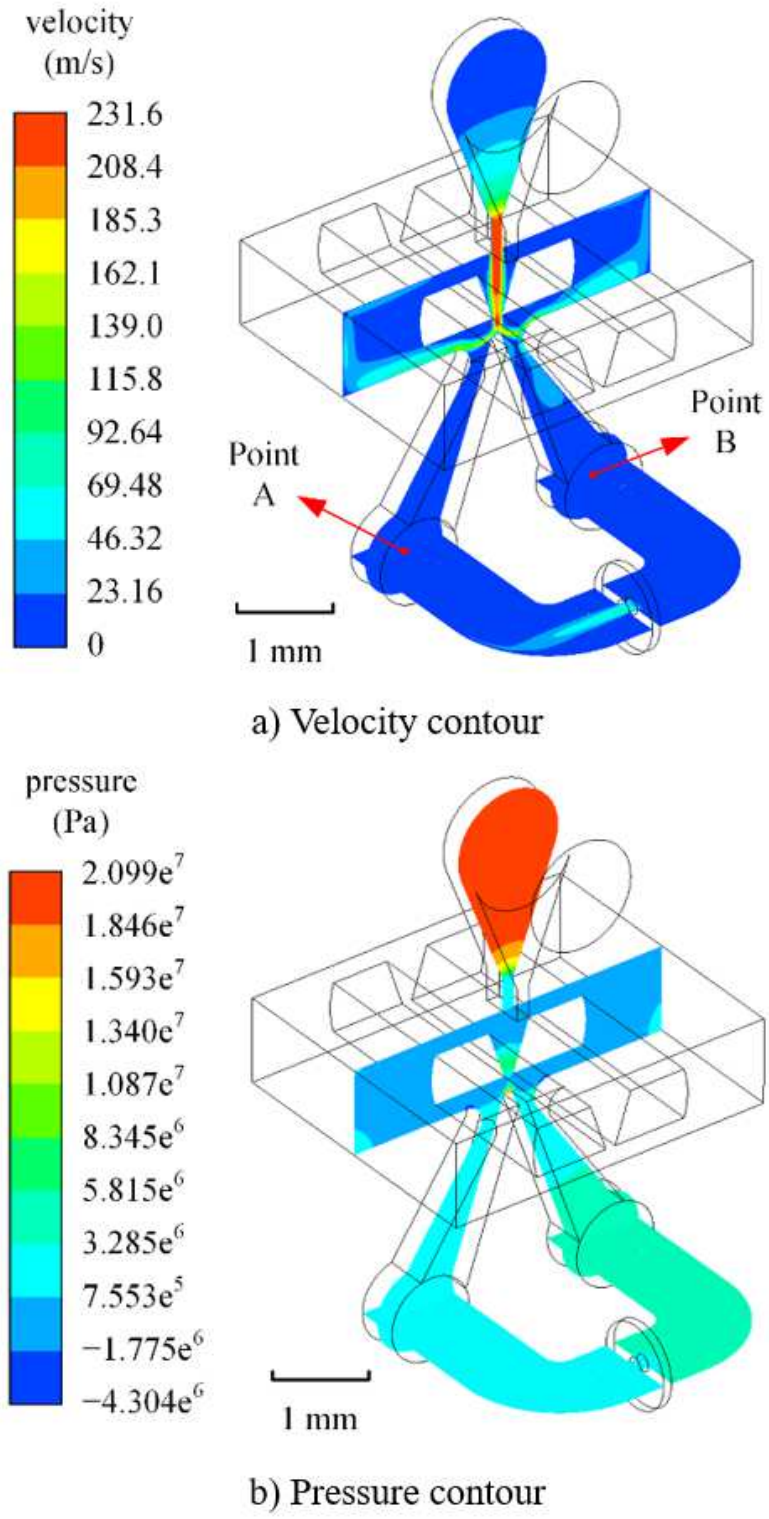

Figure 15

Simulation results of pilot stage's flow field

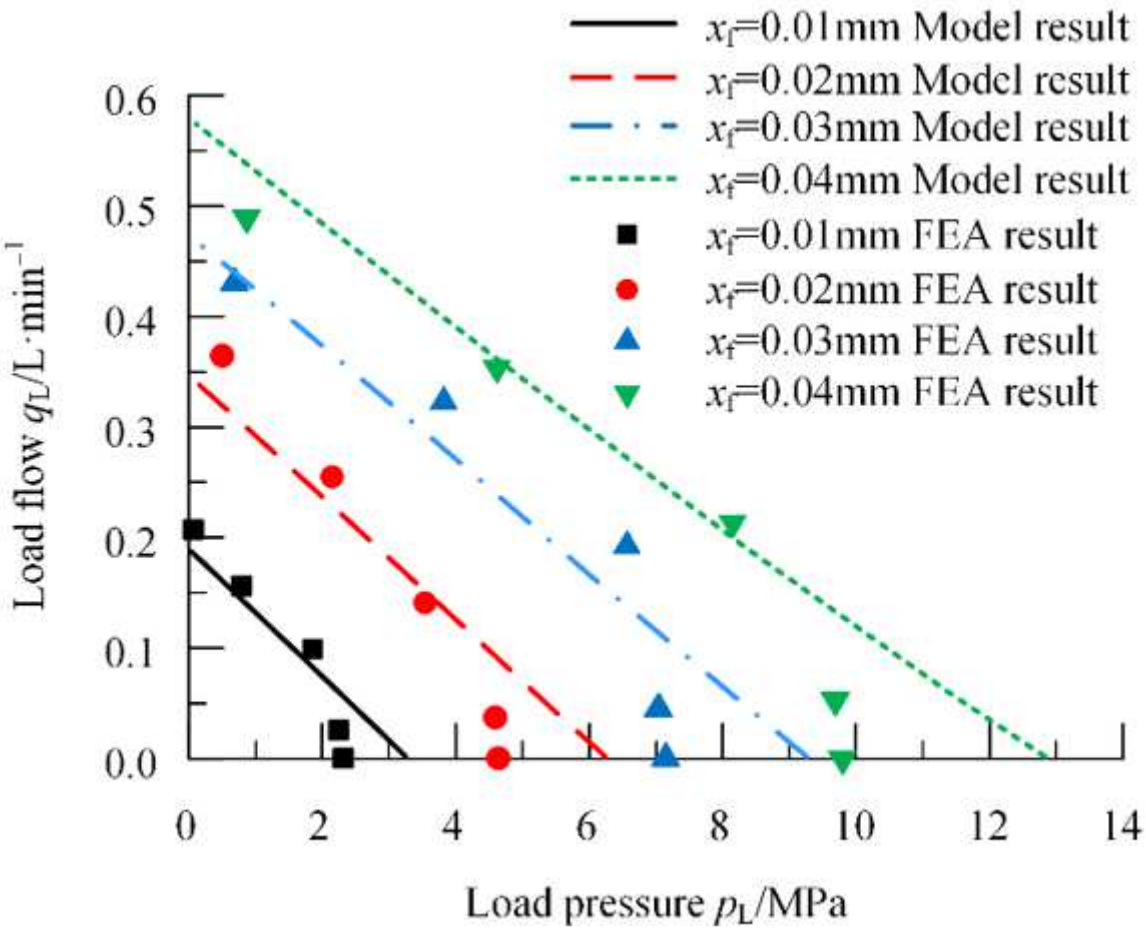

Figure 16

Pressure-flow characteristics of pilot stage compared between FEA result and model result

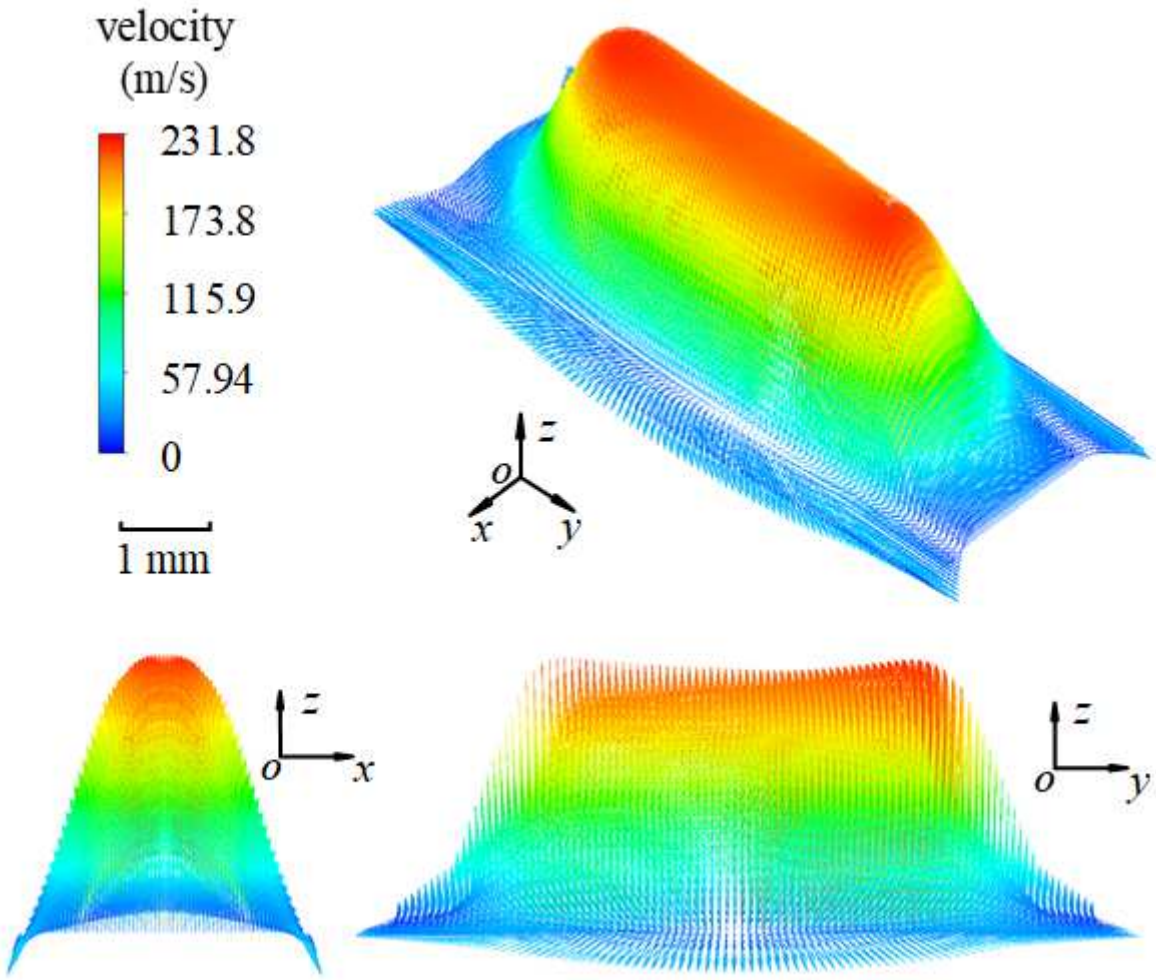

Figure 17

Velocity vector diagram of section 2-2 by FEA

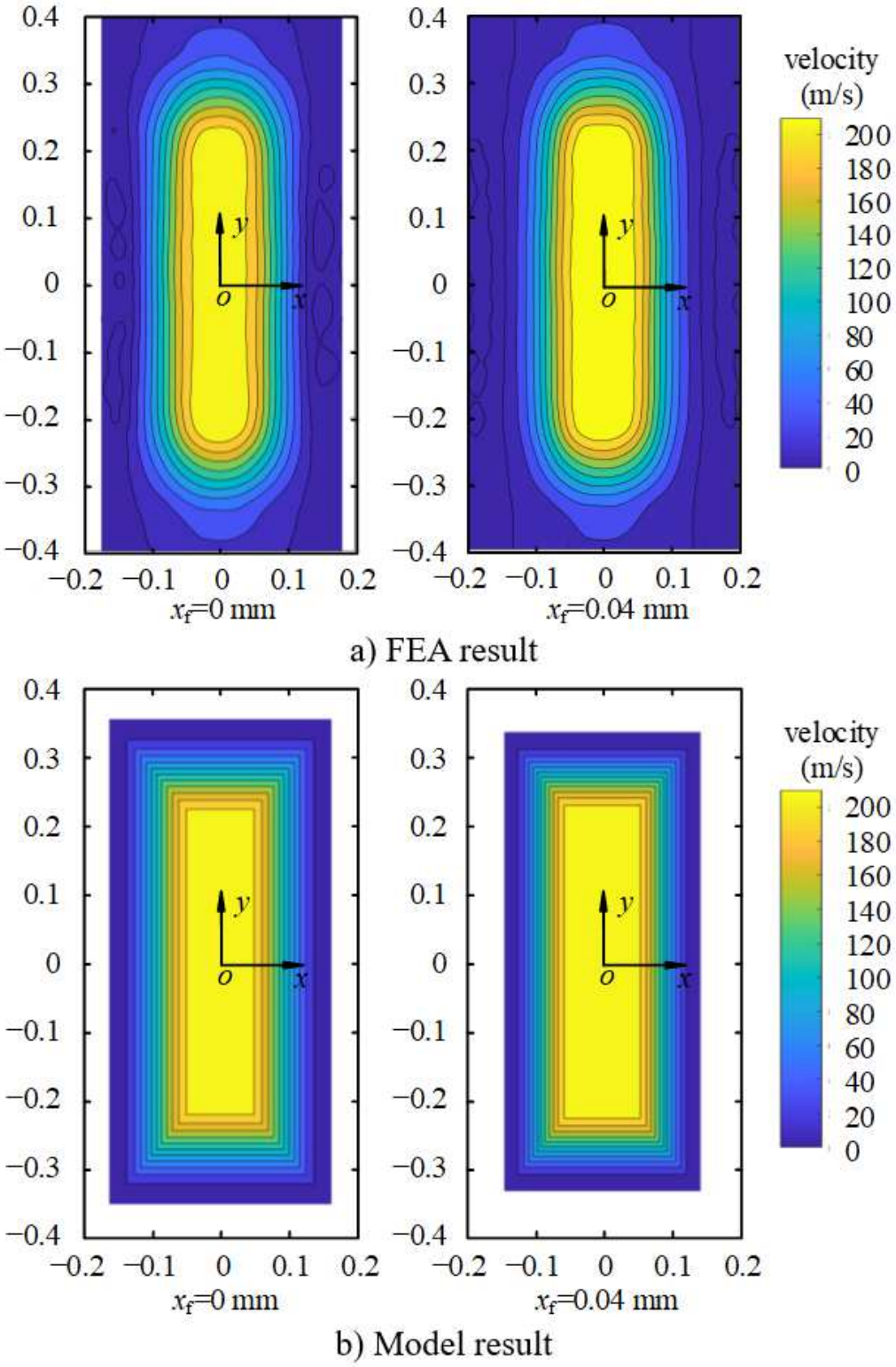

Figure 18

Velocity distribution along z direction at section 2-2

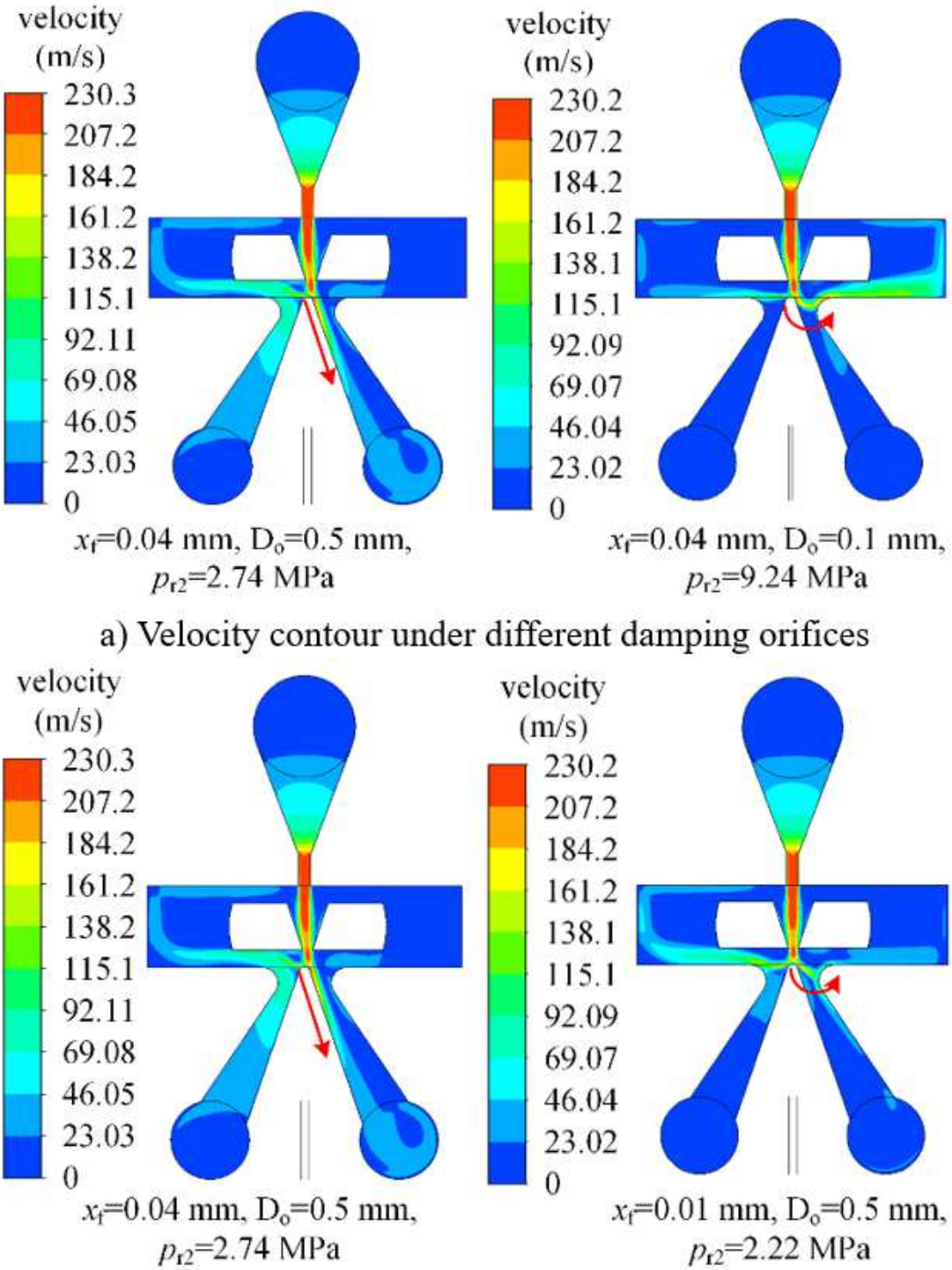

Figure 19

Jet entrainment in receiving chamber

a) Pilot stage pressure characteristics test rig

b) Photograph of jet-pan

Figure 20

Experimental setup

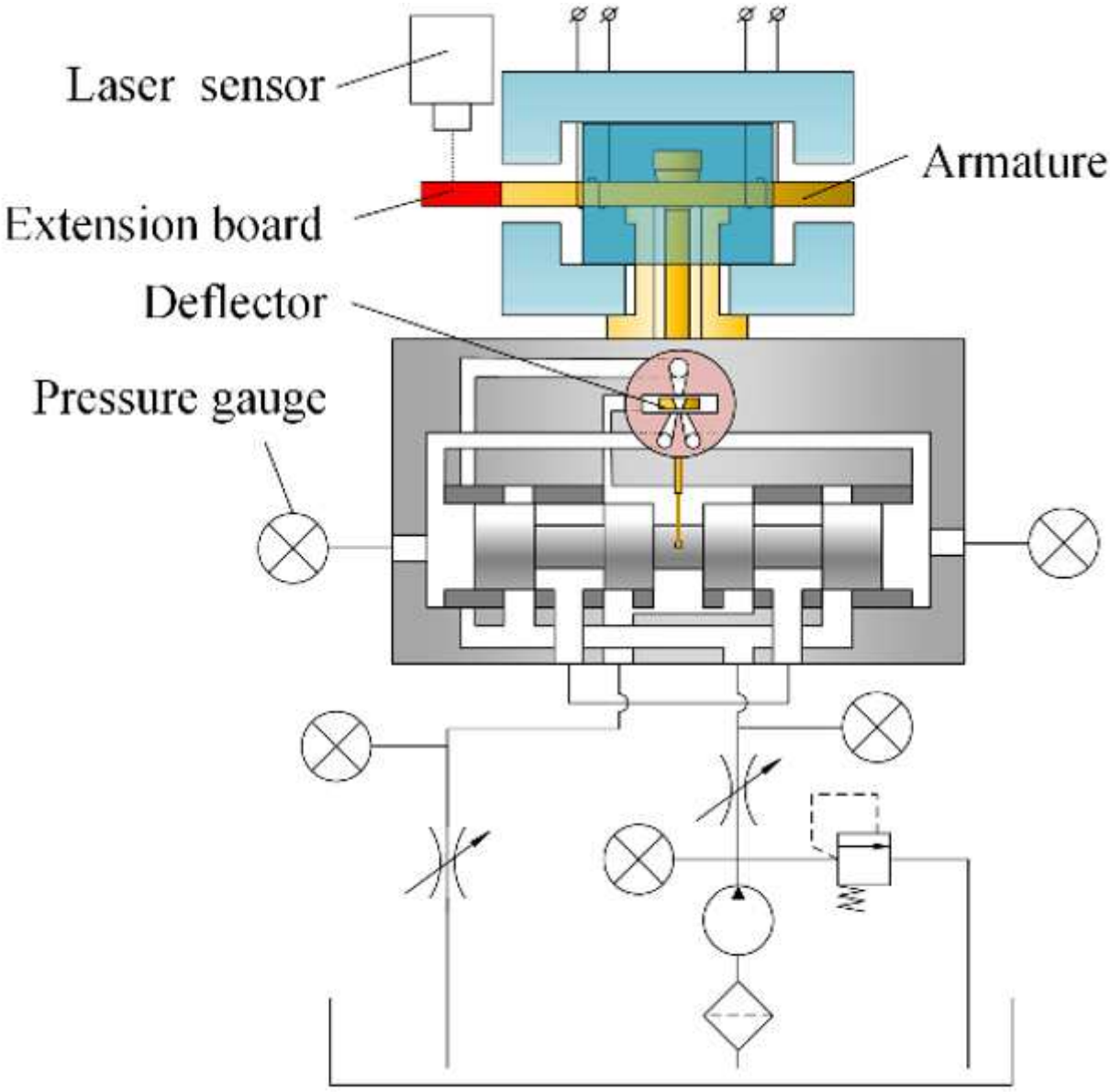

Figure 21

Schematic diagram of experimental set-up

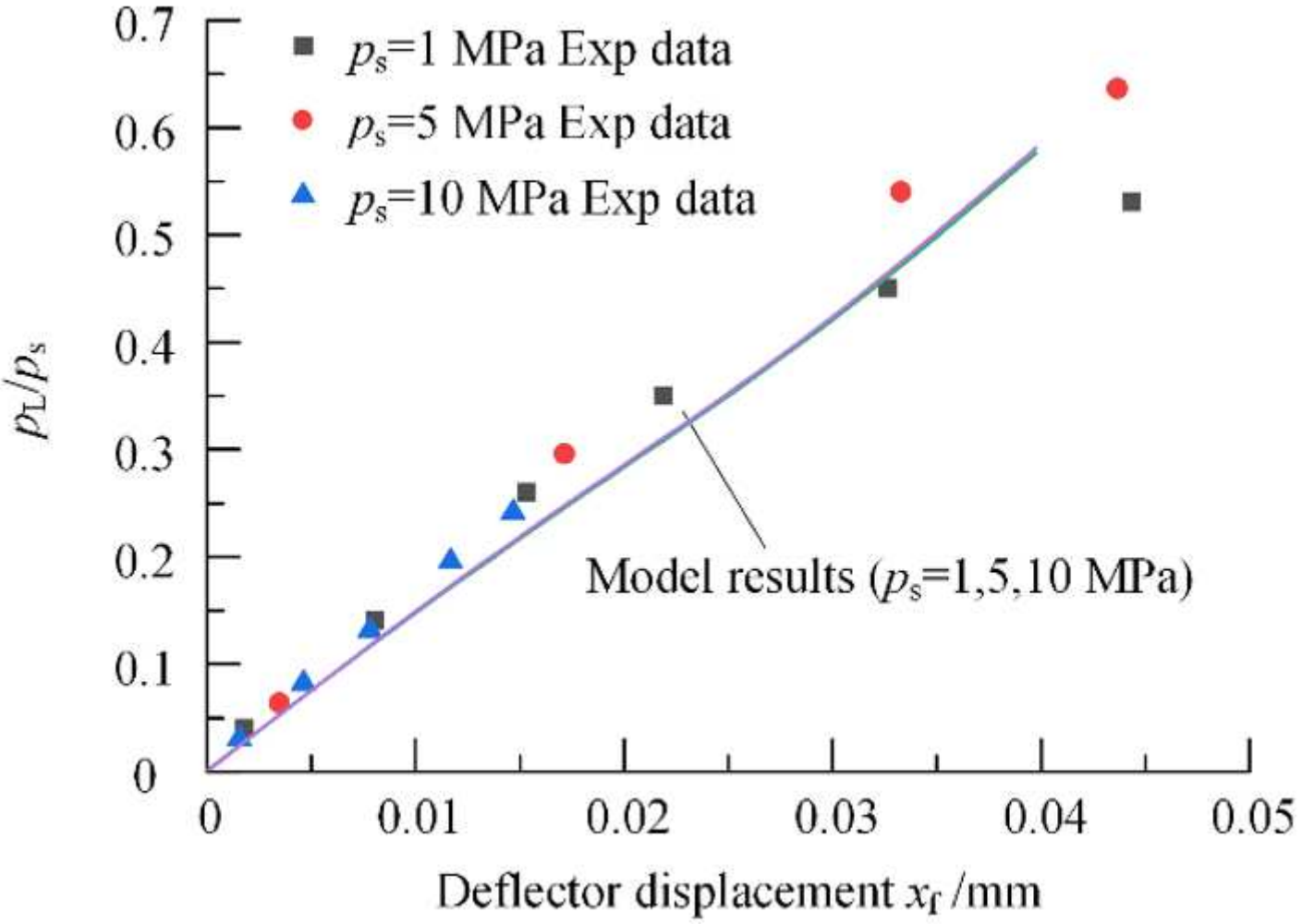

Figure 22

Dimensional cut-off load pressure characteristics